Cell Biol Toxicol (2025) 41:31
https://doi.org/10.1007/s10565-025-09988-4

RESEARCH

Innovative treatment of age-related hearing loss using MSCs and EVs with Apelin

Shengqun Xu · Dongliang Liu · Fang Zhang · Yuan Tian

Received: 5 August 2024 / Accepted: 3 January 2025

Abstract Utilizing single-cell transcriptome sequencing (scRNA-seq) technology, this study explores the viability of employing mesenchymal stem cells (MSCs) as a therapeutic approach for age-related hearing loss (ARHL). The research demonstrates MSCs' ability to differentiate into inner ear cell subpopulations, particularly hair cells, delivering Apelin via extracellular vesicles (EVs) to promote M2 macrophage polarization. In vitro experiments show reduced inflammation and preservation of hair cell health. In elderly mice, MSCs transplantation leads to hair cell regeneration, restoring auditory function. These findings highlight the regenerative capabilities of MSCs and EV-mediated therapeutic approaches for ARHL.

Keywords Mesenchymal stem cells · Age-related hearing loss · Single-cell transcriptome sequencing · Hair cell regeneration · Extracellular vesicles · M2 macrophage polarization

Shengqun Xu and Dongliang Liu these authors are regarded as co-first authors.

Supplementary Information The online version contains supplementary material available at https://doi.org/10.1007/s10565-025-09988-4.

S. Xu
Ear, Nose, Throat, Head and Neck Surgery Comprehensive Ward, Shengjing Hospital of China Medical University, Shenyang 110020, China

D. Liu · Y. Tian (✉)
Department of Otolaryngology Head and Neck Surgery, Shengjing Hospital of China Medical University, Shenyang 110004, China
e-mail: eartian@126.com

F. Zhang (✉)
Department of Otorhinolaryngology, The Fourth Affiliated Hospital of China Medical University, Shenyang 110032, China
e-mail: zhangf0285_cmu4h@163.com

Introduction

With the rapid aging of the population, the incidence of age-related hearing loss (ARHL) is gradually increasing and has become a common and serious hearing impairment (Zhao et al. 2023, Ge et al. 2023, Tajima et al. 2020). According to statistics, the adverse effects of ARHL extend beyond impacting patients' quality of life and social skills, contributing to the escalation of healthcare expenses in society (Uchida et al. 2019, Zheng et al. 2022). However, the etiology of ARHL is still unclear, and treatment strategies are relatively limited, necessitating further research (He et al. 2021, Leong et al. 2023, Cornejo-Sanchez et al. 2023).

Recent years have witnessed the emergence of mesenchymal stem cells (MSCs) as promising in the field of hearing restoration (Pouraghaei et al. 2020). With the capability to transform into diverse cell categories either in vivo or in vitro, MSCs, a form of

Published online: 17 January 2025

versatile cells, are extensively applied in the restoration and mending of tissues (Hoang et al. 2022, Bunnell 2021, Weng et al. 2022). The regulatory role of MSCs on the differentiation of inner ear-related cells has been preliminarily confirmed in previous studies, positioning MSCs as a hopeful method in managing ARHL.

A new method for exploring the causes of hearing loss has emerged with the advent of single-cell transcriptome sequencing technology, known as scRNA-seq (Koh et al. 2023, Piekna-Przybylska et al. 2023). Revolutionary improvements in scRNA-seq technology have provided a more intricate understanding of the correlation between MSCs and specific cell subpopulations in the inner ear organ of Corti (Di et al. 2021, Qin et al. 2023, Chen et al. 2022). By analyzing the results of scRNA-seq, we can further explore the differentiation mechanisms of these cell subpopulations, presenting vital clues for devising therapeutic strategies concerning ARHL (Tang et al. 2023, Hao et al. 2021, Ma et al. 2023).

The critical involvement of extracellular vesicles (EVs) in intercellular communication serves to regulate the functionality of MSCs effectively (Hade et al. 2022, Li et al. 2022). Studies have shown that Apelin in EVs has the ability to regulate the inflammatory microenvironment (Yang et al. 2023, Zhou et al. 2023). These EVs can be targeted and delivered to macrophages and exert anti-inflammatory regulatory effects, showing promise as a therapeutic avenue for managing ARHL and introducing fresh concepts to enhance treatment effectiveness for the condition (Li et al. 2023, Wei et al. 2021).

Therefore, delving into the capabilities and intricate molecular pathways of MSCs transplantation for ARHL treatment constitutes the fundamental aim of this investigation. Moreover, it seeks to illuminate the innovative approach of utilizing EVs originating from MSCs as a strategic element for combating ARHL by modulating the inflammatory context. The comprehensive grasp of these mechanisms is intended to explore novel research pathways in addressing ARHL and deliver essential guidance and utility for clinical practice. The results of this study will contribute to enhancing the well-being and social abilities of elderly individuals with hearing impairments while also providing important solutions to alleviate the burden on society's healthcare due to population aging.

Materials and methods

Sample collection for scRNA-seq analysis

Sourced from Beijing's Vital River Laboratory Animal Technology Co., Ltd. (Strain code: 219), female and male C57BL/6 mice, weighing 23 ± 2 g and aged between 6 and 8 weeks, were housed in the same cage for mating facilitation. Maintaining specific pathogen-free (SPF) conditions, all mice resided in an animal facility where the humidity ranged from 60 to 65% and the temperature was between 22 and 25℃. Unrestricted food and water were available to the mice throughout their housing. The experiments commenced after the mice had acclimated for a week, based on an evaluation of their health conditions. The Animal Ethics Committee of Shengjing Hospital at China Medical University approved the experimental procedures.

The experiment consisted of four groups ($n = 1$), namely, the E12.5 group (embryos developed to the stage of E12.5), the E18.5 group (embryos developed to the stage of E18.5), the P1 group (first day after birth), and the W6 group (6 weeks of age). Euthanasia of mice in each group took place post anesthesia, with the cochlear tissues being harvested for subsequent research endeavors (Petitpré et al. 2022).

scRNA-seq and data analysis

Surgical blades were utilized to fragment cochlear tissues extracted from individual mouse groups. Single-cell suspensions were generated from the tissues by employing trypsin (Sigma-Aldrich, 9002–07-7). The C1 Single-Cell Auto Prep System (Fluidigm, Inc., South San Francisco, CA, USA) was utilized to isolate individual cells. Lysis of the cells took place within the chip upon capture, leading to the liberation of mRNA, which was then transformed into cDNA by reverse transcription. Post lysis and reverse transcription, the cDNA underwent preliminary amplification using microfluidic chips with the aim of sequencing. Library construction and single-cell sequencing on the HiSeq 4000 Illumina platform were performed applying the pre-amplified cDNA, incorporating paired-end reads of 2×75 bp in length and an approximate read count of 20,000 reads for each cell (Mahmoudi et al. 2019).

The "Seurat" package within the R software framework was harnessed for data analysis procedures. Quality control measures were applied to the data based on the standards of 200 < nFeature_RNA < 5000 percent.mt < 20. This was followed by the identification of 2000 genes that exhibited significant variability in their expression variances (Yang et al. 2023).

The reduction in dimensionality of the scRNA-seq dataset was achieved through the utilization of principal component analysis (PCA) on the expression data of the top 2000 genes showing high variability. Utilizing the Elbowplot function within the Seurat software package, we opted for the extraction of the foremost 20 principal components (PCs) to facilitate subsequent analyses. Major cell subgroups were identified using the FindClusters function within the Seurat package at the default resolution of 1. The scRNA-seq data underwent non-linear dimensionality reduction via the application of the t-distributed Stochastic Neighbor Embedding (t-SNE) algorithm in the next stage. The Seurat tool was instrumental in pinpointing marker genes associated with distinct cell subgroups, and the "SingleR" package was employed to annotate these clusters of cells based on the marker genes (Ma et al. 2019). Additionally, pseudotime analysis was implemented using the monocle2 platform.

Cell cultivation

BLUEFBIO provided the HEI-OC1 and Ana-1 cells. The growth environment for HEI-OC1 cells involved incubation at 37 °C in a humidified incubator with 5% CO_2, utilizing high-glucose Dulbecco's Modified Eagle Medium (11,965,118, Gibco) free of antibiotics and supplemented with 10% fetal bovine serum (FBS, 10,270,106, Gibco). Passage of cells took place with the application of 0.25% trypsin/EDTA (T4049, Sigma-Aldrich) upon reaching 80% confluency. The initiation of cellular senescence was prompted in HEI-OC1 cell populations through exposure to 1 mM H_2O_2 from Sigma-Aldrich (386,790-M) over a 1-h period within 48-well cell culture dishes (Lin et al. 2019, Cho et al. 2022).

Utilizing the RPMI 1640 medium (11,875,093, Gibco), Ana-1 cells were subjected to cultivation supplemented with 10% FBS (10,270,106, Gibco) and 1% penicillin–streptomycin (15,070,063, Gibco). The 37 °C incubation of cells occurred in an environment with 5% CO_2 and humidity. To induce inflammation, the activation of Ana-1 cells was initiated by exposure to lipopolysaccharide (LPS, HY-D1056, MCE) at a concentration of 1 μg/ml for a duration of 24 h. Ana-1 cells were subjected to fluorescence labeling as per the manufacturer's guidelines, employing CellTracker™ Deep Red Dye (C34565, Invitrogen). Briefly, the treatment involved the incubation of 1.5×10^5 Ana-1 cells in a medium devoid of serum, followed by the addition of a dye solution at a concentration of 500 nM. Post a 30-min incubation, the cells received a PBS wash and were subsequently placed in 8-well chamber slides for seeding. Representative images were captured using fluorescence microscopy at 0 and 24 h after seeding CFSE-EVs (5×10^4 EVs per seeded cell) (Ragni et al. 2020).

For the isolation and culture of MSC, the leg bones of 4-week-old female C57BL/6 mice, weighing approximately 23 ± 2 g, were flushed to extract bone marrow cells. The isolated cells were then resuspended, and red blood cell lysis buffer (00–4333-57, Invitrogen) was utilized to eliminate red blood cells from the sample. The culture of about 5×10^6 cells was undertaken in α-Minimum Essential Medium (MEM α) with the addition of 9% horse serum (16,050,130, Gibco), 9% fetal bovine serum (10,270,106, Gibco), 1% Gluta-Max (35,050,079, Gibco), and 1% penicillin–streptomycin (15,070,063, Gibco). Culture conditions included maintaining the cells at 37 °C in a humidified CO_2 incubator. MSCs attached to the culture dishes were collected. A digestion process utilizing 0.25% trypsin/EDTA (T4049, Sigma-Aldrich) was executed on the cells, after which they were cultured and propagated for three rounds, with the medium renewal taking place every 3–4 days. Referred to as MSCs were these specific cells. To induce differentiation of MSCs into auditory cells, the cells were cultured with 20 ng/ml EGF (HY-P7067, MCE) and 50 ng/ml IGF-1 (HY-P70698, MCE) for 2 weeks. This was succeeded by the introduction of 10 ng/ml bFGF (HY-P7066, MCE) for an additional 2 weeks to facilitate the differentiation of MSCs (Jeon et al. 2007). To generate GFP-tagged MSC, the lentiviral expression vector pLV/puro-EF1a-GFP was introduced into MSCs through transfection facilitated by X-treme GENE HP reagent (6,366,244,001, Sigma-Aldrich) under the recommended procedures. GFP-tagged MSCs underwent

flow cytometry-based sorting after the completion of a 3-day transfection (Wang et al. 2018).

Cell grouping and transfection

To establish cell lines with gene silencing or overexpression, we employed lentiviral transduction. These included MSCs with knockdown of Apelin (sh-Apelin) and their corresponding control cell line (sh-NC), as well as MSCs with overexpression of Apelin (oe-Apelin) and their control cell line (oe-NC). Two sets of shRNA sequences were concurrently tested for a knockdown, and the more effective set was chosen for subsequent experiments. Table 1 illustrates the lentiviral sequences implemented for the silencing of genes. Shanghai Bioscientific (China) offered plasmids and lentiviral packaging solutions.

The initiation of lentivirus-mediated cell transfection involved the seeding of 1×10^5 cells into a 6-well plate. The transfection process commenced when the cellular density reached 70–90%, with the introduction of a medium containing an adequate dose of enclosed lentivirus (MOI = 10, operational concentration around 1×10^6 TU/mL) and 5 μg/mL polybrene (TR-1003, Sigma-Aldrich). An equivalent medium volume was incorporated after 4 h to alleviate the polybrene concentration, and a fresh medium exchange occurred after 24 h. Stable transduced cell lines were established through resistance screening with 1 μg/mL puromycin (A1113803, Thermo Fisher) following a 48-h transfection (Zhi et al. 2021, Gao et al. 2022).

β-galactosidase staining

To determine cellular senescence, the Cell Senescence β-Galactosidase Staining Kit (C0602, Beyotime) was utilized as directed by the manufacturer for assessment. The seeding of cells took place in a 6-well culture dish. Following a gentle wash with PBS, each well was treated with 1 mL of fixation solution for β-galactosidase staining, and then fixed at room temperature for 15 min. Subsequent to the triple PBS washes, 1 mL of the staining working solution was administered to every well containing the cell samples. Overnight incubation at 37 °C without CO_2 was conducted in the 6-well plate, which had been meticulously covered with foil. Microscopic observation was performed, and 5 fields of view in the center and periphery were counted and averaged (Cho et al. 2022).

Table 1 Lentiviral transfection sequence

Name	Sequence (5'−3')
sh-NC	TTCTCCGAACGTGTCACGT
sh-Apelin-1(Mouse)	CCTTACTCTTTGAGGTCATAT
sh-Apelin-2(Mouse)	AGAAGAAGGAAGCATGCGCTA

CCK-8 assay

The CCK-8 assay kit (CK04, Dojindo Laboratories) was applied for the analysis of cell viability. The seeding density of cells in a 96-well plate was set at 1×10^5 cells per well. Each well received 10 μL of CCK-8 solution daily, with subsequent addition of 100 μL of serum-free medium. An incubation period of 2 h at a temperature of 37 °C was allowed for the plate, followed by measuring the optical density (OD) at a wavelength of 450 nm. Viability of cells was assessed by the formula % = [(experimental well—blank well)/(control well—blank well)] × 100% (Ma et al. 2019).

ELISA assay

The ELISA kits were employed to measure the concentrations of IL-10 (IL-10, CUSABIO), Arg1 (CSB-EL002005MO, CUSABIO), IL-1β (CSB-E08054m, CUSABIO), and IL-6 (ab222503, Abcam) in the cell culture supernatant. First, the antigens were diluted to appropriate concentrations and added to the wells of an enzyme-labeled reaction plate. Then, the enzyme-labeled antibodies and substrate solution were applied to the plate, incubated, and followed by the introduction of 50 μL stop solution to halt the reaction, with the experimental outcomes assessed in a span of 20 min. The ELISA reader (1,681,135, Bio-Rad, USA) was utilized for reading the plate's absorbance at 450 nm. After plotting a standard curve, thorough analysis was conducted on the obtained data (Yun et al. 2021). All assays were conducted following the manufacturer's guidelines. Each sample was tested in triplicate to ensure result accuracy.

Acridine orange (AO) staining

Cell viability was determined using AO staining solution (CA1143, Soleibao). The experimental procedure was conducted according to the instructions provided by the reagent. Initially, two PBS washes were administered to the gathered cells. Subsequently, the number of cells was tallied and modified to a density of 1×10^6/ml. The infusion of AO dye (1 mg/ml) into the cell suspension led to a concentration of 10 μg/ml. Post a 15-min incubation under light exclusion at room temperature, the stained cells underwent observation under a fluorescence microscope (with an excitation filter set at 488 nm and an emission filter at 515 nm) in order to compute cellular vitality. Apoptotic cells appeared orange, while viable cells appeared green. Five fields of view were observed in both the center and periphery and the average values were obtained (Niknazar et al. 2019). Each experiment was replicated thrice.

Collection, preparation, and depiction of EVs

MSC groupings received two PBS washes and were subsequently exposed to FBS-free MDEM after incubation. The supernatant was gathered after a span of 48 h, then centrifuged to separate cells and debris. At a temperature of 4 °C, the centrifugation process involved steps at 300 g for 10 min, 2000 g for 20 min, and 10,000 g for 30 min. A 1-h exposure at 37 °C was employed for the labeling of cells with 10 μM CFSE (65–0850-84, Invitrogen). Ultracentrifugation at 4 °C and 100,000 g for a period of 3 h was performed to isolate CFSE-labeled EVs. Following the removal of any extra dye, the EVs that had been collected underwent a washing process with PBS and were then reconstituted in PBS. To ensure the purity of the isolated EVs sample, we evaluated the ratio between the number of microvesicles and the total amount of protein. Only when the ratio fell within the range of 10^8–10^{10} particles/μg protein did we consider the EVs batch to have high purity (Ragni et al. 2020, Liu et al. 2020).

Fluorescently labeled EVs (CFSE-EVs) underwent examination through a CytoFLEX flow cytometer (Beckman Coulter, USA) prepared with FITC-fluorescent beads for calibration. This enabled the identification of fluorescent particles with a size as minute as 100 nM. Standard beads of 160, 200, 240, and 500 nM (Biocytex) were used for calibration. EVs were diluted in PBS at a 1:10,000 ratio and stained with CD63-APC (143,905, Biolegend) and CD81-APC (104,909, Biolegend) antibodies. A 30-min staining procedure was conducted at a temperature of 4 °C. Post-staining, the samples underwent dilution in PBS to 1,000 μL for assessment with the flow cytometer.

To establish a gating strategy for selecting only the stained EVs, CFSE-EVs were compared to PBS + CFSE samples in the FITC channel. Events within this gate were used for subsequent analysis. The purpose of this step was to exclude antibody aggregates that produced spontaneous fluorescence in the FITC channel, ensuring that only CFSE-labeled EVs were analyzed. Subsequently, CFSE-positive EVs were detected using the flow cytometer (Ragni et al. 2020).

Nanoparticle tracking analysis (NTA)

Dilution in PBS at a 1:100 ratio was applied to the EV samples. The diluted EV samples were then placed in the Nanosight LM10-HS system (Malvern Panalytical). For each EV sample, a 30-s video recording was conducted to capture the movement trajectory of EV particles in PBS (Ragni et al. 2020). The experiment was repeated three times.

Atomic force microscopy (AFM)

Firstly, the collected exosomes were diluted in PBS and then dropped onto pre-prepared glass slides. Subsequently, the samples were air-dried overnight at room temperature. Next, high-resolution images of the exosomes were prepared using an AFM and an ACT cantilever in semi-contact mode (Bagheri et al. 2020).

Transmission electron microscopy (TEM)

10 μL of EV suspension was fixed in 4% paraformaldehyde and drop-casted onto formvar carbon-coated EM grids for air-drying. Subsequently, it was stained with 3% phosphotungstic acid (G1871, Soleibao) for 5 min. Finally, the morphology of EVs was thoroughly observed and analyzed using a JEOL 1010 TEM (JEOL) (Yang et al. 2023).

Immunofluorescence (IF) staining

The cells obtained were treated with 4% paraformaldehyde (P0099, Beyotime) for a duration of 15 min and then rinsed thrice in PBS. The cochlear tissues of mice, post-embedding, underwent slicing into slices of 8 μm, cleansing with PBS on slides arranged in advance, and then fixation with 4% paraformaldehyde lasting 10 min per slide to boost the adhesion of the tissue to the glass material. Post three subsequent PBS washes, cells or sections of the cochlea were subjected to hindering by a mixture including 0.3% Triton X (BL935B, Biosharp), 1% bovine serum albumin (V900933, Sigma-Aldrich), and 10% serum from goats (C0265, Beyotime) for an interval of 30 min. Overnight incubation at 4 °C involved treating the slides with the primary antibodies provided: Prestin (PA5-103,158, 1/100, ThermoFisher), Arg-1 (ab137614, 1:100, abcam), Myo7a (ab150386, 1/100, Abcam), Sox2 (ab92494, 1/100, Abcam), Iba1 (ab178846, 1/200, Abcam), Na–K ATP (A11683, 1/200, ABclonal), Atoh1 (PA5-29,392, 1/100, Invitrogen), CD206 (MA5-16,871, 1/100, Invitrogen), CD80 (MA5-15,512, 1/200, Invitrogen), and Cx26 (71–0500, 1/100, Invitrogen). Upon completion of three PBS rinses, the slides were subjected to a 2-h incubation at room temperature in the absence of light, with the addition of secondary antibodies: goat anti-rabbit IgG (H + L) Alexa Fluor® 488 (ab150077, 1/200, Abcam), Alexa Fluor® 594 (ab150080, 1/200, Abcam), or Alexa Fluor® 647 (ab150083, 1/200, Abcam). The staining of F-actin involved the use of Alexa Fluor® 647-conjugated phalloidin (A22287, 1:200, sourced from Invitrogen) and incubated for 30 min at ambient temperature. Upon conclusion of the experimental steps, the slides underwent a thorough wash with PBS before being affixed using an anti-fade mounting compound infused with DAPI (4083, CST). Subsequent observations and image capture were performed utilizing a laser scanning confocal microscope (LSM 980, ZEISS) (Yang et al. 2022, Takeda et al. 2021). Five animals were assigned to each group, and the cochlear tissue of each animal was stained on a singular slice, with an individual field of view designated for imaging. The cellular studies were redone on three occasions. ImageJ software from the National Institutes of Health in the USA was employed to estimate the proportion of positive cell density subsequent to imaging.

Real-time quantitative reverse transcription polymerase chain reaction (RT-qPCR)

Extraction of total RNA from cellular samples in the various groups was accomplished through the application of the Trizol reagent (T9424, Sigma-Aldrich). A UV–visible spectrophotometer (ND-1000, Nanodrop, USA) was employed to measure the quality and concentration of RNA. The mRNA expression analysis entailed the implementation of reverse transcription with the PrimeScript™ RT reagent kit (RR014B, TaKaRa, Japan). The performance of RT-qPCR was executed via an ABI 7500 PCR apparatus (Applied Biosystems, USA), with the utilization of the TB Green® Premix Ex TaqTM reagent kit (RR420W, TaKaRa, Japan). The internal control for mRNA was GAPDH. Employing the comparative Ct method for relative quantification, the fold change in target gene expression in the experimental group as opposed to the control group was represented using the formula $2^{-\Delta\Delta Ct}$, where ΔΔCT = ΔCt experimental group—ΔCt control group, and ΔCt = target gene Ct—internal control gene Ct (Yang et al. 2023).

Western blot (WB)

The protein extraction kit (BC3710, Solarbio, China) was applied for the extraction of total cellular or tissue proteins. Centrifugation of the supernatant was carried out at 13,000 rpm for 15 min at a temperature of 4 °C. Utilizing the BCA protein quantitation kit (P0010, Beyotime, China) allowed for the determination of protein levels. A PVDF membrane was used for the transfer of proteins following their separation by SDS-PAGE electrophoresis. Blocking the membrane involved the utilization of 5% skim milk at ambient temperature for a duration of 60 min. Addition involved diluting the primary antibodies listed below: Apelin (PA5-114,860, 1/1000, ThermoFisher), Prestin (PA5-103,158, 1/1000, ThermoFisher), Atoh1 (21,215–1-AP, 1/1000, ThermoFisher), Sox2 (ab92494, 1/1000, Abcam), Myo7a (ab150386, 1/1000, Abcam), p53 (ab26, 1/1000, Abcam), p21 (ab109199, 1/1000, Abcam), Arg-1 (ab203490, Abcam), IL-10 (ab310329, Abcam), and GAPDH (ab8245, 1/5000, Abcam). Anti-Rabbit-IgG secondary antibody (7074, 1/1000, CST) or Anti-Mouse-IgG secondary antibody (7076, 1/1000, CST) was then added and incubated at ambient temperature for 1 h.

The membrane underwent three wash cycles applying TBST solution (each lasting for 5 min). Removal of TBST was followed by preparation of an adequate volume of ECL working solution (WBULS0500, EMD Millipore, USA). The PVDF membrane was introduced into the ECL developing solution for soaking and then kept at room temperature for 1 min. Elimination of excess ECL operating solution from the PVDF film, enclosing the film with plastic wrap, placing it in a dark storage, and allowing a 5–10 min exposure for the development and fixing (Wang et al. 2021). Quantitative grayscale analysis of the WB bands was achieved by employing the ImageJ software, with GAPDH serving as the internal reference.

Flow cytometry

Preparation for flow cytometry-based cell surface marker analysis involved isolating MSCs with 0.25% trypsin/EDTA (T4049, Sigma-Aldrich) and placing them in PBS supplemented with 3% FBS. Under a cold condition of 4 °C, cells were treated with specific antibodies for staining: anti-CD11b-PE (553,311), anti-CD34-PE (551,387), anti-CD29-PE (562,801), anti-CD45-PE (567,111), anti-CD90-PE (551,401), anti-CD105-PE (562,759), anti-CD146-PE (562,196), anti-Sca-1-PE (561,077), anti-CD80-APC (560,016), and anti-F4/80-APC (566,787) purchased from BD Biosciences. Anti-CD63-APC (17–0631-82), anti-CD81-FITC (MA5-17,939), anti-CD206-APC (17–2061-82), and anti-CD163-PE (12–1631-82) were purchased from Invitrogen. Finally, each group's cells underwent two PBS washes, were sorted via a flow cytometer (Beckman Coulter, USA), and analyzed utilizing the FlowJo software (Liu et al. 2020).

Animal experiments, MSCs transplantation, and EVs treatment

CBA/CaJ (000654) male mice were purchased from Jackson Laboratory, including young (8–10 weeks old) and old (18–19 months old) mice. The entire mouse population was housed in a facility that met SPF standards, where the humidity was controlled within 60–65% and temperatures were maintained between 22–25 °C, with water freely available. A one-week acclimation period was provided for the mice before the experiment, with careful observation of their health status. The institutional committee responsible for animal ethics approved the experimental procedures and protocols for animal usage (Seicol et al. 2022).

For MSCs transplantation: Anesthetized mice were positioned on a warming mat to regulate their body temperature. The skin in the area behind the left ear, where the procedure was performed, was disinfected with 1% iodine solution. The untreated control was implemented on the right ear. By utilizing a Leica M205A stereomicroscope, a slice of 0.5 cm was initiated on the rear aspect of the left ear, and the subcutaneous muscle was dissected to expose the temporal bone. Next, the utilization of forceps allowed for the exposure of the round window vicinity by opening the left ear canal, and the diameter of the opening was expanded to facilitate the visualization of the round window membrane (RWM). The delivery of MSCs suspension into the Scala tympani of the ear through the RWM was accomplished by employing a Picoliter microinjection system (PLI-100A, Warner Instrument) from a glass pipette within a 1 to 2-min timeframe. Approximately 0.5 μL (1×10^7 cells/mL) of cell suspension was injected into the cochlea. Upon withdrawal of the pipette, a tiny fragment of muscular or adipose tissue obtained from the neck region was promptly positioned above the puncture area to prevent any leakage from the circular window site. Closure of the auditory sac orifice involved the application of 6–0 absorbable chromic sutures, after being concealed by adipose tissue. Post the treatment, the animals were reinstated within their enclosures for staying (Takeda et al. 2021).

For EV treatment: Administration of EVs. sh-NC or EVs.sh-Apelin, both at a concentration of 60 μg/mL, via tail vein injections was conducted on a cohort of 5 mice for a continuous duration of 4 weeks (Li et al. 2021).

The assessment of auditory brainstem response (ABR) and distortion product otoacoustic emissions (DPOAE) values was performed at intervals of 7, 14, and 28 days post MSCs engraftment or EV treatment in the respective mouse groups. The mice were euthanized on the 28th day of the trial through cervical dislocation while under general anesthesia, and tissue specimens were gathered for subsequent experiments (Li et al. 2021).

ABR

In this study, administering pentobarbital sodium intraperitoneally at a dose of 50 mg/kg was used to induce anesthesia in mice. The body temperature of 37 °C was sustained through the application of a heating pad. Upon initiating the test, a 1/4-inch microphone (PCB-378C01, PCB Piezotronics) was placed on the ears of the experimental animals. Additionally, three silver wire electrodes were inserted: an active electrode between the ears at the cranial vertex, a reference electrode beneath the right ear, and a ground electrode in the midline of the back. During the experiment, stimuli of different tones including 2, 4, 8, 16, and 32 kHz were delivered at a rate of 21.1 kHz per second. The BioSigRZ software (TDT, USA) was employed for capturing the animals' responses. Starting at 90 decibels sound pressure level (dB SPL) for the initial stimulation intensity, it was subsequently diminished in 5 dB increments until achieving the threshold level. The threshold was designated as the minimum level of sound intensity required for observing visually identifiable and replicable wave patterns (Sun et al. 2022).

DPOAE

This investigation involved the measurement of 2f1-f2 DPOAE responses through the implementation of the real-time signal processing system II developed by Tucker-Davis Technologies (TDT, USA). The output stimulus was calibrated using ABR measurements to ensure accurate measurements. The primary stimulus signals (f1 and f2) were set at two intensity levels, specifically L1 = 80 dB SPL and L2 = 75 dB SPL, with an f2/f1 ratio of 1.22. DPOAE response thresholds were recorded at multiple frequency ranges, including 2, 4, 8, 16, and 32 kHz. The DPOAE recordings were executed by employing two separate speakers to emit the primary tones, along with the utilization of a low-noise microphone, ER 10B (Etymotic Research, USA). In DPOAE analysis, only when the peak of the 2f1-f2 spectral component exceeded the background noise level by more than 3 dB was it considered a valid DPOAE response (Sun et al. 2022).

Methods for analyzing data and statistical software

Our research involved the application of R language version 4.2.1 via the integrated development interface RStudio, version 2022.12.0–353. The utilization of GraphPad Prism 8.0 was instrumental in processing all data. Demonstrative data was exhibited in the format of Mean ± SD, denoting the mean with standard deviation. The utilization of non-paired t-tests was essential for the evaluation of two datasets, whereas one-way analysis of variance (ANOVA) was pivotal for investigating differences among multiple datasets. Levene's test was utilized to evaluate the equality in variances. Pairwise comparisons underwent Dunnett's T3 and LSD-t tests provided that variances showed homogeneity; however, in the absence of homogeneity in variances, the Dunnett's T3 test was employed. The statistical significance level was established at $P < 0.05$, revealing meaningful distinctions across the analyzed groups (Zhang et al. 2020).

Results

Identification of cell types in mouse cochlea development using scRNA-seq analysis

In order to investigate the cellular and molecular mechanisms related to hearing degeneration in the cochlear structures of mice at different developmental stages, we conducted scRNA-seq analysis. We collected cochlear samples from three different developmental stages: Embryo group (E12.5, E18.5), Young group (P1), and Adult group (W6) (Fig. 1A). The information underwent processing and consolidation via the Seurat software toolkit. Firstly, we examined the gene count (nFeature_RNA), mRNA molecule count (nCount_RNA), and percentage of mitochondrial genes (percent.mt) for all cells in the scRNA-seq data. Most cells were characterized by nFeature_RNA < 5000, nCount_RNA < 20,000, and percent.mt < 20% (Fig. S1A). We filtered out low-quality cells using a criteria of 200 < nFeature_RNA < 5000 percent.mt < 25%, culminating in an expression dataset including 17,453 genes and 19,963 cells.

Next, examination of sequencing depth correlation unveiled that post filtration, the data exhibited a correlation coefficient of r = −0.04 between nCount_RNA and percent.mt, and a correlation

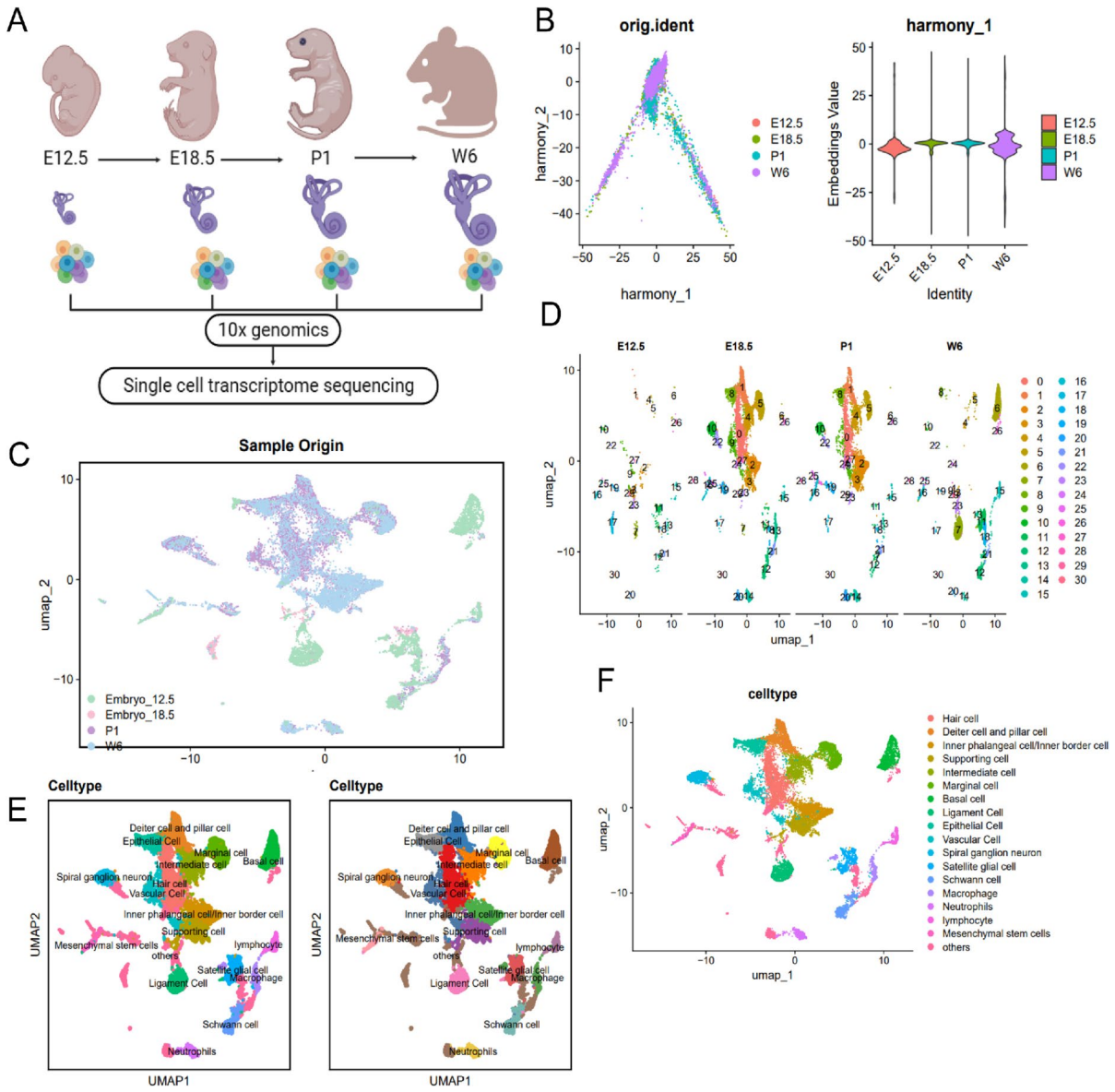

Fig. 1 Cell clustering and annotation of scRNA-seq data. Notes: **A** scRNA-seq analysis was performed on samples collected from Embryo (E12.5 and E18.5 stages), P1 (postnatal day 1) and W6 (6 weeks old) mice, $n=1$; **B** Distribution of cells in PC_1 and PC_2 after batch correction using Harmony, where each point represents a cell; **C** Visualization of UMAP clustering results, showing the clustering and distribution of cells from embryo (E12.5 and E18.5), P1, and W6 cochlear samples in two-dimensional space; **D** Visualization of UMAP clustering results, showing the clustering and distribution of cells from different sources, where each color represents a cluster; **E** Visualization of UMAP clustering results, showing the cell types and distribution in the cochlea of different source samples, where each color represents a cluster; **F** Visualization of cell annotation results based on UMAP clustering, where each color represents a cell cluster

coefficient of r = 0.89 between nCount_RNA and nFeature_RNA (Fig. S1B), signifying good quality of the filtered cell data for further analysis.

In order to delve deeper into the examination of the screened cells, we opted to pick out genes with significant variation in their expression levels.

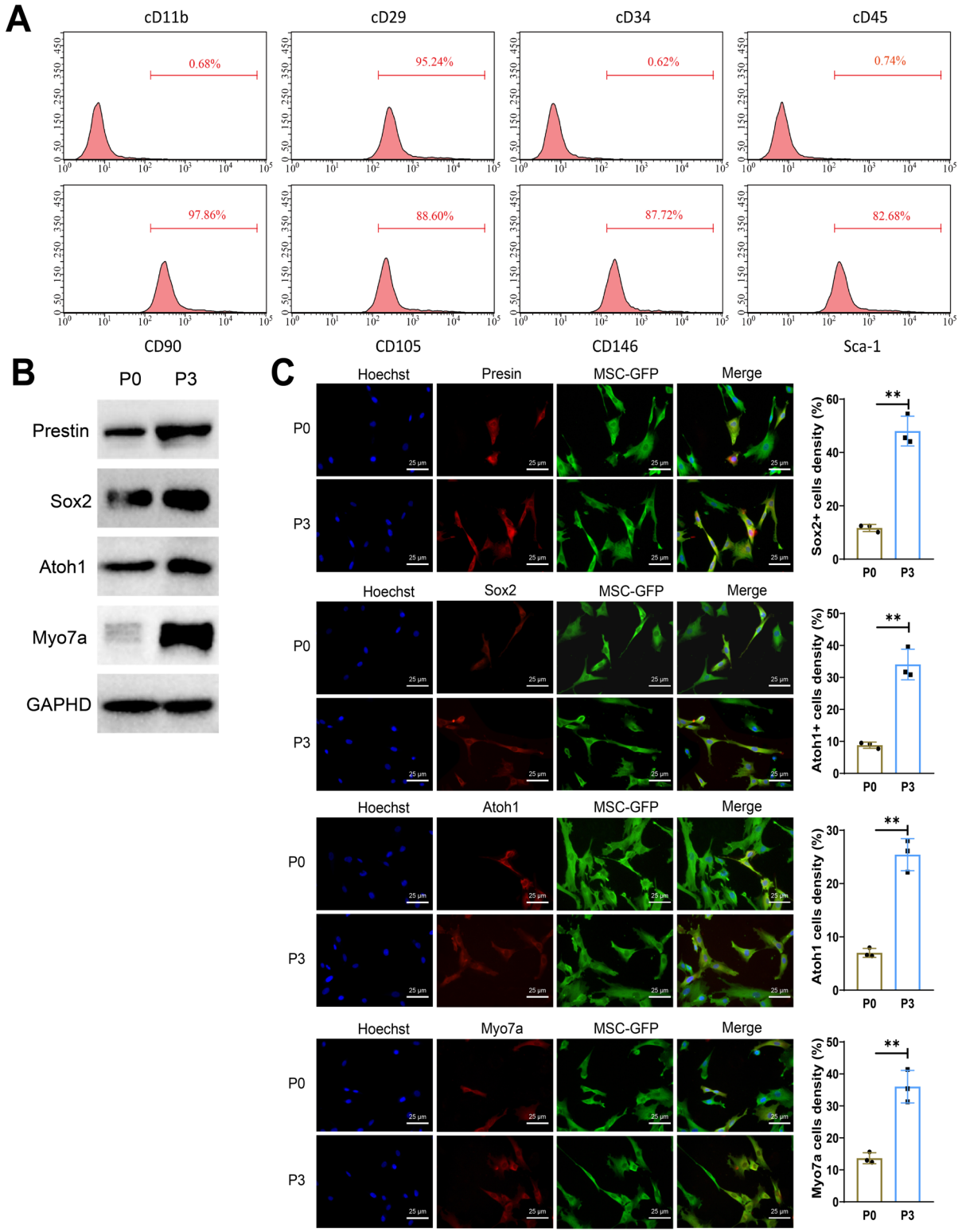
A
cD11b
cD29
cD34
cD45
0.68%
95.24%
0.62%
0.74%
97.86%
88.60%
87.72%
82.68%
CD90
CD105
CD146
Sca-1
B
P0
P3
Prestin
Sox2
Atoh1
Myo7a
GAPHD
C
Hoechst
Presin
MSC-GFP
Merge
Sox2
Atoh1
Myo7a
P0
P3
25 μm
Sox2+ cells density (%)
Atoh1+ cells density (%)
Atoh1 cells density (%)
Myo7a cells density (%)
**

◂**Fig. 2** Differentiation of MSCs into auditory-related cells. Notes: **A** Flow cytometry analysis of MSCs derived from bone marrow, labeled with fluorescent markers $CD11b^+$, $CD29^+$, $CD34^+$, $CD45^+$, CD90, $CD105^+$, $CD1146^+$, and Sca-1; **B** Expression levels of Prestin, Sox2, Atoh1, and Myo7a detected by WB; **C** IF staining to assess the expression of Sox2 and Atoh1. $^{**}P<0.01$, three independent cell experiments were performed

Subsequently, we picked the foremost 2000 genes with remarkable variability for subsequent analysis (Fig. S1C). The initial normalization of data followed the completion of cell cycle scoring facilitated by the CellCycleScoring function (Fig. S1D). Linear dimensionality reduction of the dataset involved applying PCA. Demonstrated here is the heatmap representing the primary gene expression interactions of PC_1-PC_6 (Fig. S1E) and the cell distribution in PC_1 and PC_2 (Fig. S1F), pointing toward the occurrence of batch influences among the samples.

Implementing batch correction with the harmony tool, we aimed to minimize batch effects and enhance the precision of cell clustering within the dataset (Fig. S1G). The ElbowPlot was applied to rank the standard deviation of the PCs, with the findings indicating that PC_1-PC_20 sufficiently depicted the data originating from the highly variable genes, showcasing notable analytical relevance (Fig. S1H). The corrected findings pointed out the successful eradication of batch effects across the samples (Fig. 1B).

In addition, application of the UMAP algorithm led to non-linear dimension reduction for the top 20 PCs. The utilization of UMAP clustering led to the acquisition of 31 distinct cell clusters (Fig. 1C-D). We then used the Bioconductor/R package "SingleR" for automatic annotation of these 31 cell clusters, resulting in 17 different cell types (Fig. 1E-F), including cells located in the organ of Corti (Hair cell, Deiter cell and pillar cell, Inner phalangeal cell/Inner border cell, Supporting cell), cells in the Stria vascularis (Intermediate cell, Marginal cell, Basal cell), cells in the Spiral ligament (Ligament cell, Epithelial cell, Vascular cell), cells in the Modiolus (Spiral ganglion neuron, Satellite glial cell, Schwann cell), and different types of immune cells (Macrophage, Neutrophils, Lymphocyte).

In summary, the scrutiny of cochlear tissue development in mice at different temporal stages led to the successful identification of 31 cell clusters, delineating a total of 17 cell classifications through our scRNA-seq analysis.

Key role of MSCs in auditory cell differentiation revealed by scRNA-seq analysis

Based on scRNA-seq analysis, we observed variations in the composition of cochlear cells at different stages of development. MSCs, which are non-hematopoietic multipotent stem cells, possess self-renewal and differentiation abilities into mesodermal tissues such as adipocytes, chondrocytes, and osteocytes. The trend of evidence suggests that MSCs show promise in differentiating into neurons and sensory cells (Jeon et al. 2007). Therefore, from the aforementioned scRNA-seq analysis, we extracted the MSCs population (Fig. S2A) and annotated the hair cells, Deiter cells, pillar cells, and inner phalangeal cells/inner border cells in the organ of Corti (Fig. S2B-D). These findings reveal the correlation between MSCs and the differentiation of auditory-related cells.

Exploring the differentiation stage of MSCs in depth, we utilized pseudotime analysis using the R tool monocle2 to map out the course of MSCs differentiation. Initially, visualization of sorted genes was performed, as depicted in Fig. S3A. Subsequently, DDRTree was implemented for data dimensionality reduction, facilitating the sorting of cells based on gene expression trends, thereby establishing a differentiation trajectory (Fig. S3B). The evolution of MSCs can be divided into five stages, including two significant branching points, according to different states (Fig. S3C-D). Pseudotime, calculated by monocle2 based on the gene expression information of cells, is used to represent the temporal order of cells (Fig. S3E). We observed that MSCs are more concentrated in the Stat1 stage and play an essential role throughout the differentiation process (Fig. S3F).

Based on the aforementioned scRNA-seq analysis, we discovered the association of MSCs with the differentiation of auditory-related cells. The literature suggests that MSCs exhibit differentiation potential towards inner ear auditory cells when cultured in the presence of IGF-1, EGF, and bFGF (Jeon et al. 2007). To further validate our findings, MSCs were isolated from bone marrow, and flow cytometry was employed to detect surface markers of MSCs. The results indicated high expression levels of CD29, CD90, CD105, CD1146, and Sca-1 in MSCs, while CD11b, CD34,

and CD45 were negative (Fig. 2A). After confirming the specific surface markers of MSCs, cultivation of MSCs took place in a serum-free solution including IGF-1, EGF, and bFGF. Examination of cochlear sensory progenitor cell-related factors was carried out using WB at the third phase of in vitro cultivation. The detection results showed upregulation of Prestin, Sox2, Atoh1, and Myo7a expression levels in the P3 group in relation to the P0 group (Fig. 2B). Furthermore, IF staining indicated a substantial escalation in the number of Sox2 + and Atoh1 + positive cells generated by MSCs-GFP in the P3 group relative to the P0 group (Fig. 2C).

To summarize, this research unveiled the crucial role of MSCs in the differentiation process of auditory functional cells through scRNA-seq and pseudotime analysis. Our results not only confirm the important role of MSCs in cochlear development but also provide critical information for the maturation of auditory function.

Examination of the ability of MSCs to regenerate auditory hair cells revealed by transplantation study

The primary reason for hearing impairment usually stems from the demise of sensory cells in the cochlea, resulting in significant adverse effects on individuals' everyday activities. Since hair cell death is not spontaneously regenerated in mammals, rescuing hair cell regeneration holds promise as a key strategy for treating sensorineural hearing loss. Pluripotent stem cells represent a potential therapeutic approach whereby they can be transplanted into the cochlea of hearing loss patients to differentiate into otic progenitor cells and inner ear hair cells, thus restoring hearing function (Chen et al. 2012).

Firstly, we utilized phalloidin staining to demonstrate the state of the cochlear cell cytoskeleton in the Young and Old groups. IF staining results revealed a disrupted cytoskeleton in the cochlear tissues of the Old group in contrast with the Young group (Fig. S4A). Additionally, the expression levels of Myo7a-positive cells were downregulated in the cochlear tissues of the Old group contrasted against the Young group (Fig. S4B).

We transplanted MSCs into the lymph periphery of Old group mice, using GFP-labeled MSCs to track their migration and differentiation within the mice's inner ears (Fig. 3A). The inner ear consists of three major parts (Fig. 3B): the scala vestibule (SV), the scala media (SM), and the scala tympani (ST). The elements consist of hair cells, sensory cells, the spiral ligament, blood vessels regulating the SM cochlear potential, and primary auditory neurons or spiral ganglion neurons (Kanzaki et al. 2020). Using fluorescent labeling with Myo7a and Sox2, which represent inner ear hair cells and auditory progenitor cells, respectively, we found that migratory MSCs were detected in the SV, SM, and ST regions, generating GFP + Sox2 + Myo7a + cells, further indicating the differentiation of MSCs into hair cell progenitor cells (Fig. 3C). By day 28, MSCs were also detected in the organ of Corti's Apex region, differentiating into Myo7a +, Sox2 +, and Sox2 + Myo7a + cells, as shown by IF labelin (Fig. 3D).

The experimental findings point towards the potential efficacy of MSCs in renewing cells linked to auditory functions within the cochlea.

Improved hearing function and increased expression of connexin and ion channels following MSCs transplantation

We investigated the impact of MSCs transplantation on hearing using ABR and DPOAE evaluations. The ABR and DPOAE hearing thresholds demonstrated no statistically significant disparities within the initial week post MSCs transplantation. However, over time, particularly in the second and fourth weeks, there was a significant decrease in ABR and DPOAE hearing thresholds, indicating an improvement in auditory function (Fig. 4A-B).

The levels of Cx26 and Na–K ATP expression within the squamous epithelium (SE) of the tympanic membrane (TM) were investigated. Functioning significantly within the cochlear tissue of the inner ear, Cx26 acts as a crucial intercellular connectivity protein. Cx26 protein facilitates the transfer of ions and small molecules between cells through channels connecting adjacent cells. Normal cochlear function relies heavily on the presence of Cx26 expression in the cochlea, which is crucial for establishing the link between the outer hair cells and the supporting cells (Sanchez and Verselis 2014).

Within the structures of the inner ear, the Na–K ATP ion channel protein holds fundamental importance in regulating the physiological processes of the cochlear tissue. This channel is responsible for

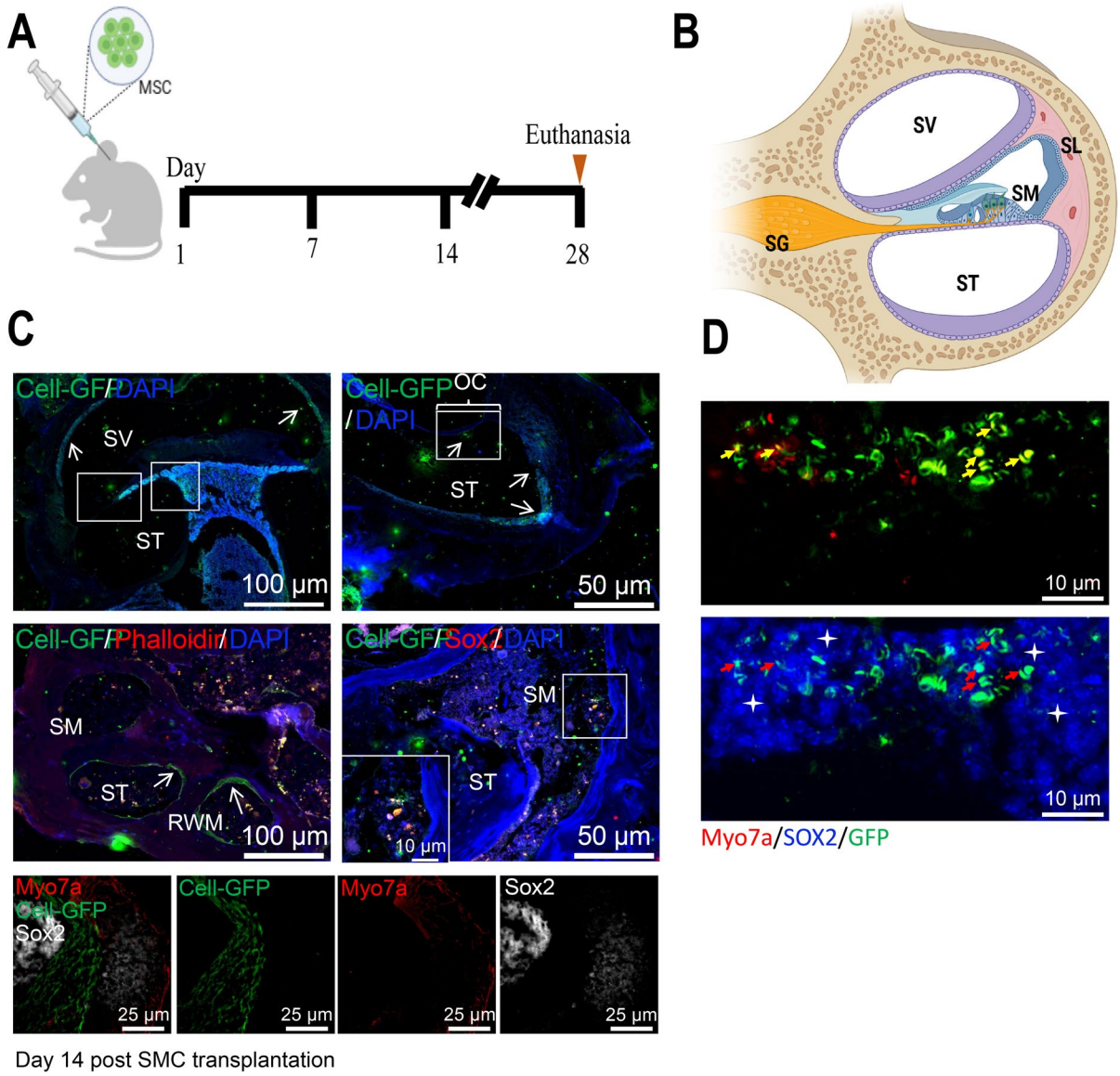

Fig. 3 Expression profile of MSCs in the cochlear tissue after transplantation. Note: **A** Schematic diagram of the in vivo experiment, illustrating the transplantation of GFP-labeled MSCs into the cochlear tissue of Old mice, with the evaluation of MSC's effects on auditory function at different time points; **B** Schematic diagram of the mouse inner ear structure: SM represents Scala media, ST represents Scala tympani, and SV represents Scala vestibul; **C** Top panel: IF detection of the cochlear vestibule and middle ear at day 14 post-MSCs transplantation. Green indicates MSC-GFP, red indicates Sox2, and blue indicates DAPI. White arrows point to migrated MSCs. Bottom panel: Magnified view of GFP + Sox2 + Myo7a + positive cells; **D** IF detection of GFP^+Sox2^+ and GFP^+Myo7a^+ cell expression in the Apex region 28 days after MSCs transplantation. Yellow arrows indicate GFP^+Myo7a^+ positive cells; asterisks indicate GFP^+Sox2^+ positive cells, and red arrows indicate $GFP^+Sox2^+Myo7a^+$ positive cells

regulating the membrane potential of cells, especially outer hair cells, to help maintain normal auditory system function (Holm and Lykke-Hartmann 2016). IF results showed a significant upregulation of Cx26 and Na–K ATP expression in the cochlear tissue after MSCs transplantation (Fig. 4C). These findings provide molecular-level evidence for the improvement of auditory function with MSCs transplantation and

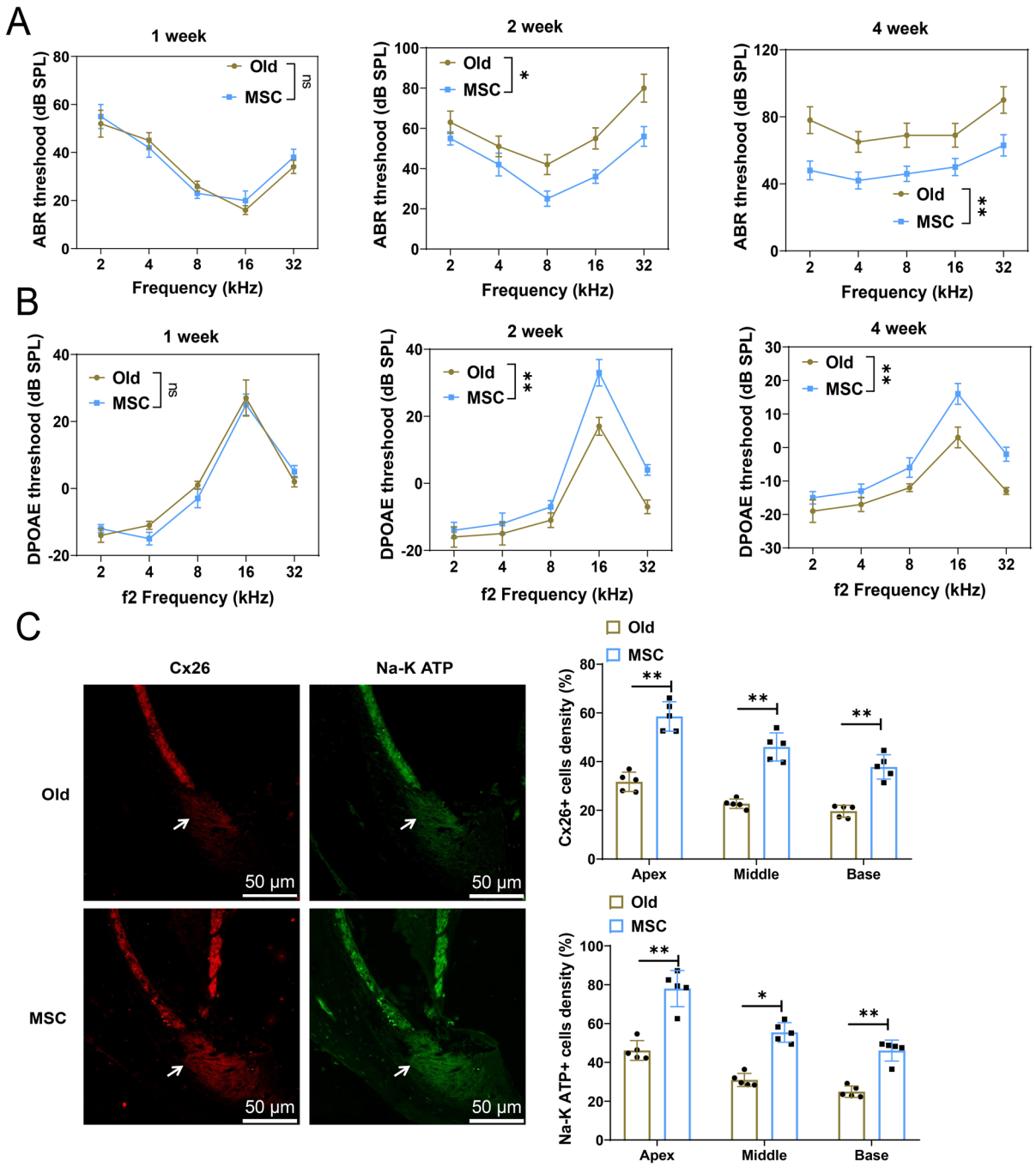

Fig. 4 Improved auditory function in aged mice after MSCs transplantation. Note: **A** Evaluation of ABR hearing thresholds in different groups of mice at various time intervals after MSCs transplantation; **B** Assessment of DPOAE hearing thresholds in different groups of mice at different time intervals following MSCs transplantation; **C** IF staining to examine the expression of Cx26 and K^+-ATPase α. Scale bar = 50 μm. $^{**}P < 0.01$, $^{*}P < 0.05$, ns $P > 0.05$, $n = 5$

suggest that MSCs may enhance and maintain inner ear function by promoting the expression of the connectivity proteins Cx26 and Na–K ATP.

ARHL: the role of macrophage activation and the potential of MSCs therapy

ARHL, also known as presbycusis or age-related deafness, is a common issue that gradually develops with age. In recent years, inflammation has been a key area of investigation in biomedical research concerning age-related diseases. As tissues age, the body undergoes a phenomenon called "chronic inflammation." A pivotal function of the immune system involves inflammation, which is essential in combatting infections and injuries (Watson et al. 2017, Gruver et al. 2007). However, chronic or excessive inflammatory responses may have a negative impact on the auditory system (Verschuur et al. 2014). In the cochlea, macrophages, as long-lived resident immune cells, have a fundamental function in modulating local inflammatory responses. Depending on their activation state, they can either promote or suppress acute inflammatory reactions in the cochlear microenvironment (Liu et al. 2018). Studies have found a high aggregation of macrophages in the cochlea of ARHL patients (Noble et al. 2019).

Thus, we further investigated the changes in macrophages within the ear tissue during the aging process in mice. IF analysis revealed that, in contrast with the Young group, the Old group showed a marked growth in the number of activated macrophages (Iba1) and M1 macrophages (CD80-positive cells), a marked decrease in M2 macrophages (Arg-1-positive cells), and a reduced proportion of Myo7a-positive cells (Fig. 5A).

In assessing how MSCs affect the macrophage phenotype, macrophages (Ana-1) were treated with LPS and co-cultured with MSCs. The ELISA findings indicated increased levels of IL-6 and IL-1β, which are markers for M1 macrophages, and a decrease in IL-10 and Arg-1, which serve as markers for M2 macrophages, when comparing the LPS group to the Control group; however, the levels of these factors were dynamically changed by MSCs in a time-sensitive manner, differing from those in the LPS group (Fig. 5B). Additionally, the flow cytometry technique was employed to determine the levels of M1 and M2 macrophages. The outcomes indicated an escalation in the percentage of M1 macrophages and a reduction in the percentage of M2 macrophages observed in the LPS group in relation to the Control group; meanwhile, MSCs reversed the levels of expression of these cells in contrast to the LPS group (Fig. 5C).

To conclude, our experiments suggest a correlation between the activation of macrophages and ARHL. However, MSCs therapy has the potential to decrease macrophage activation and the secretion of inflammatory factors, thus improving the overall well-being of the auditory system.

MSC-derived EVs regulate macrophage activation in inflammatory response

The above studies and experimental results indicate that MSCs therapy has the potential to inhibit macrophage activation. Moreover, MSC-derived EVs carry a wealth of anti-inflammatory molecular information, including anti-inflammatory proteins, miRNAs, and RNAs, which can influence the physiological state and immune responses of recipient cells (Baglio et al. 2015). Moreover, their capacity lies in the control over immune cell polarization, changing pro-inflammatory M1 macrophages to anti-inflammatory M2 macrophages, thus aiding in the reduction of inflammation (Cao et al. 2019). Therefore, we propose that MSCs mediate macrophage activation through the release of EVs.

In our study, we first evaluated the morphology, uniformity, and size of EVs from MSCs using AFM (Fig. S5A). Further validation of EV size was conducted using TEM (Fig. S5B). The use of calibrated flow cytometry confirmed the size range of EVs, indicating that over 98% of EVs are smaller than 200 nm (Fig. S5C). Additionally, we detected the expression of EV markers CD63 and CD81 using flow cytometry (Fig. S5D-E).

To simulate the inflammatory microenvironment of macrophages, we stimulated Ana-1 macrophages with LPS and subsequently treated them with different concentrations of EVs. IF outcomes indicated a substantial escalation in the proportion of M2 macrophages in a concentration-dependent manner after EV treatment (Fig. 6A). We also collected cell supernatant and performed ELISA to assess the expression of M1 macrophage markers (IL-6 and IL-1β) and M2 macrophage markers (IL-10 and Arg1). Significantly reduced IL-6 and IL-1β

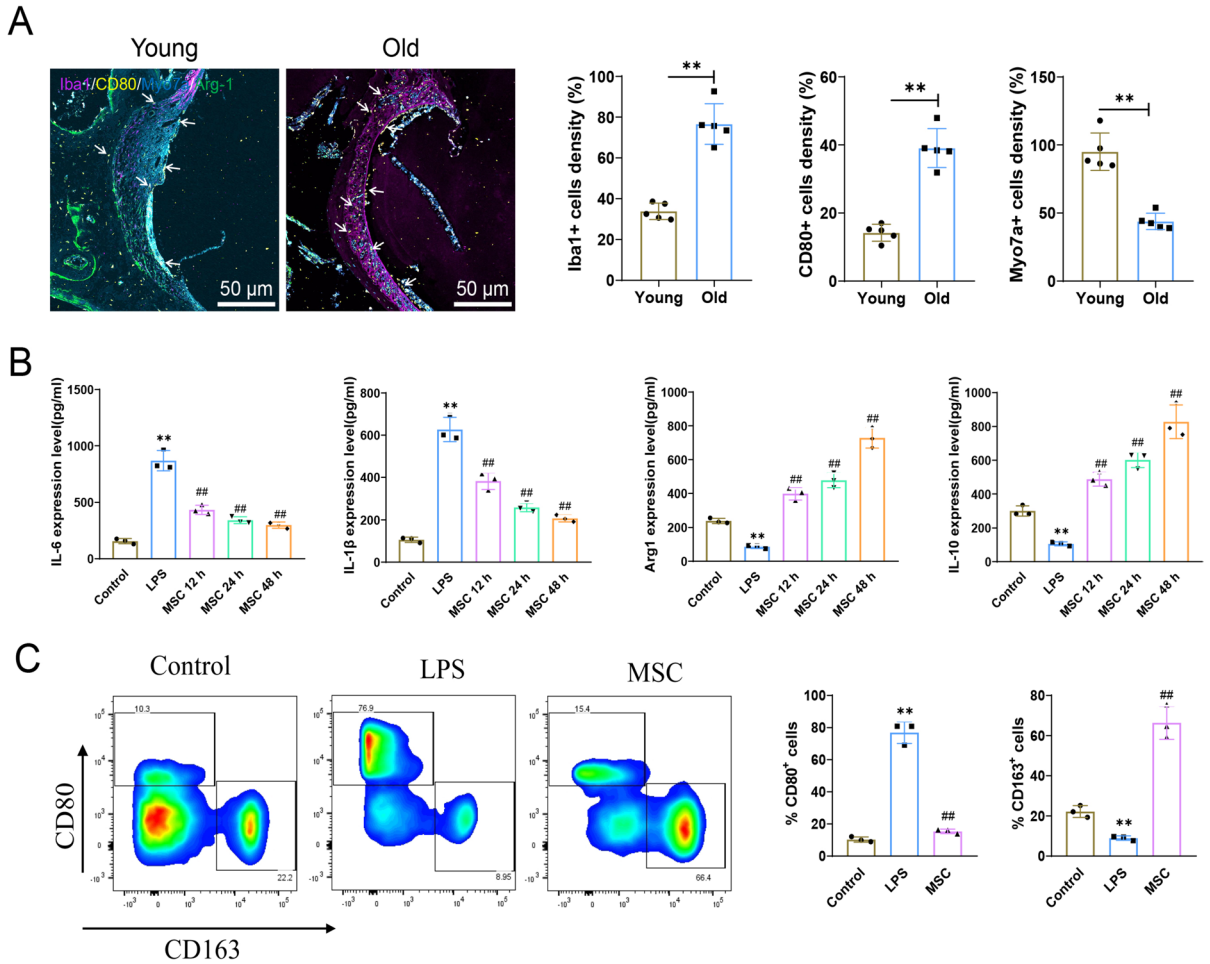

Fig. 5 MSC-mediated inhibition of inflammatory response in macrophages. Note: **A** IF detection of Iba1, CD80, and Myo7a expression in cochlear tissue of Young and Old mice, with white arrows indicating CD80-positive cells. Scale bar = 50 μm; **B** Stimulation of Ana-1 macrophages with LPS (1 μg/ml) in co-culture with MSCs, followed by ELISA analysis of IL-6, IL-1β, Arg1, and IL-10 expression in the cell supernatant at different time points; **C** Flow cytometry analysis of M1 macrophages ($CD80^+$) and M2 macrophages ($CD163^+$) after co-culturing MSCs with Ana-1 macrophages for 48 h. $^{**}P<0.01$, $^{*}P<0.05$ compared to Control group; $\#\#P<0.01$ compared to LPS group. Animal experiments were $n=5$, and cell experiments were repeated 3 times

expression along with markedly elevated IL-10 and Arg1 expression were observed with the escalation of EV concentration according to the findings (Fig. 6B-E).

EVs, as a class of small membrane-bound vesicles, are released into the extracellular environment to regulate intercellular communication and signaling by carrying bioactive molecules. The modulation of immune responses and the facilitation of cell communication are primary functions of EVs in the immune system. Serving as essential intermediaries, they facilitate the interaction and communication between macrophages and a multitude of other immune cells (Hu et al. 2021).

Therefore, our experiments further investigated the interaction between EVs and macrophages. Flow cytometry illustrated a noteworthy surge in the fluorescence intensity of macrophages over time, suggesting their propensity for CFSE positivity and showing a distinct shift in fluorescence peaks (Fig. 6F). IF staining results demonstrated the presence of CFSE-labeled EVs in the cytoplasm of macrophages, indicating specific and ordered interactions between EVs and macrophages (Fig. 6G).

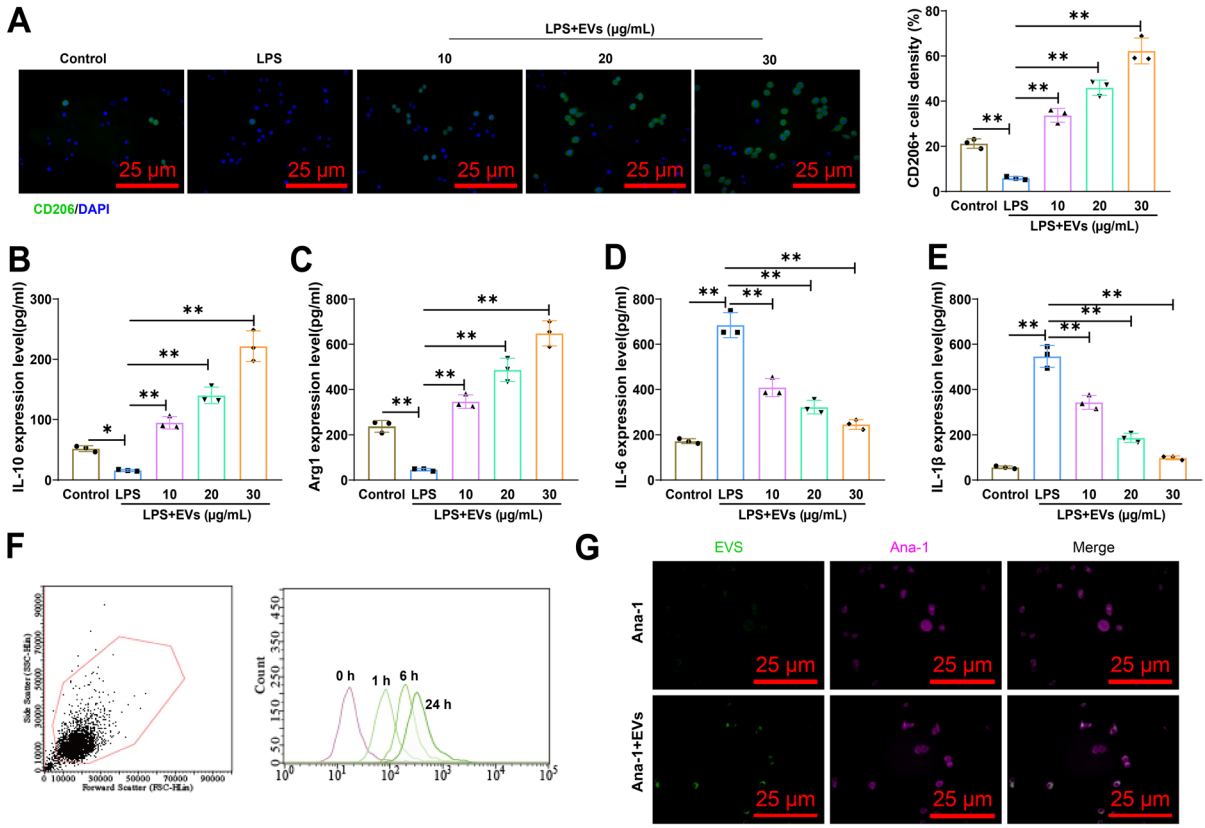

Fig. 6 EVs derived from MSCs suppress the occurrence of inflammatory response. Note: **A** Stimulation of Ana-1 macrophages with LPS (1 μg/ml) and treatment with EVs at different concentrations for 24 h, followed by IF detection and quantification of M2 macrophages ($CD206^+$). Scale bar = 25 μm; **B-E** ELISA analysis of IL-6, IL-1β, IL-10, and Arg1 expression in the cell supernatant after treating macrophages with different concentrations of EVs for 24 h; **F** Flow cytometry analysis of fluorescence intensity of macrophages ($F4/80^+$) after co-culturing them with CFSE-stained EVs for 0, 1, 6, and 24 h; **G** IF staining of macrophages (highlighted in magenta) and EVs (highlighted in green) using CellTracker™ Deep Red dye, showing the interaction between macrophages and EVs. White arrows indicate merged images of EVs interacting with macrophages. Scale bar = 25 μm. $^{**}P < 0.01$, $^{*}P < 0.05$, cell experiments were repeated 3 times

These results suggest that EVs derived from MSCs may play a role in suppressing inflammatory responses by modulating the activation status of macrophages.

Apelin-mediated MSC-derived EVs promote M2 polarization in inflammation

Apelin is an endogenous peptide hormone that has been extensively studied for its role in inflammation. External stimuli often lead to inflammation, prompting the activation of immune cells and the release of inflammatory mediators as part of the body's defense response. Recent investigations have elucidated the vital function of Apelin in regulating inflammatory responses. By activating the APJ receptor, apelin has the capability to suppress the generation of inflammatory agents and the stimulation of immune cell function (Wang et al. 2022). This includes inhibitory effects on inflammatory cells comprising macrophages and T cells, thereby alleviating the severity of the inflammatory response. Additionally, Apelin facilitates the enhancement of anti-inflammatory cellular activities, particularly macrophages engaged in inflammation resolution, thereby contributing to the reinstatement of inflammatory balance (Leeper et al. 2009).

To investigate the expression of Apelin in EVs, we retrieved data from the exoRBase database. The heatmap and line graph showed that the Apelin

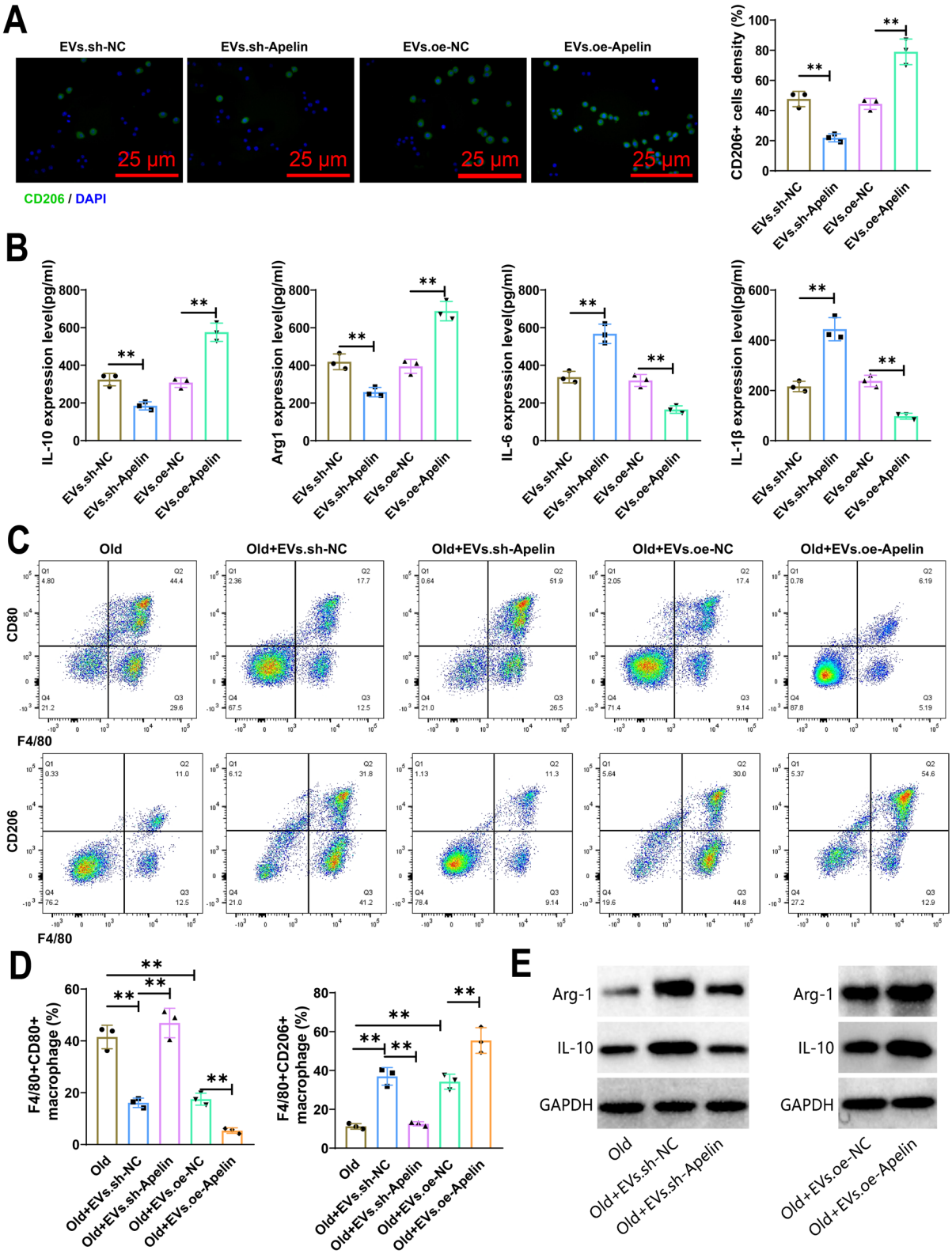
A
EVs.sh-NC
EVs.sh-Apelin
EVs.oe-NC
EVs.oe-Apelin
25 μm
CD206 / DAPI
CD206+ cells density (%)
B
IL-10 expression level(pg/ml)
Arg1 expression level(pg/ml)
IL-6 expression level(pg/ml)
IL-1β expression level(pg/ml)
C
Old
Old+EVs.sh-NC
Old+EVs.sh-Apelin
Old+EVs.oe-NC
Old+EVs.oe-Apelin
CD80
CD206
F4/80
D
F4/80+CD80+ macrophage (%)
F4/80+CD206+ macrophage (%)
E
Arg-1
IL-10
GAPDH

◂**Fig. 7** EVs mediate anti-inflammatory effects through Apelin delivery. Note: **A** Transduction of MSCs with Apelin lentivirus, either with silenced or overexpressed conditions, followed by collection of EVs released by these MSCs and co-culturing with macrophages. IF staining was performed to detect the expression of M2 macrophage marker CD206. Measurement of the scale bar = 25 μm; **B** Expression of IL-6, IL-1β, IL-10, and Arg1 in the cell supernatant was measured using ELISA; **C-D** Expression of M1 ($F4/80^+CD80^+$) and M2 ($F4/80^+CD206^+$) macrophage markers in cochlear tissue was assessed using flow cytometry; **E** Expression levels of Arg-1 and IL-10 in cochlear tissue were detected by WB. $^{**}P < 0.01$, $^{*}P < 0.05$, cell experiments were repeated 3 times

expression level was relatively higher in EVs secreted by embryonic stem cells (ESSCs) (Fig. S6A-B). Furthermore, our investigation focused on the expression of Apelin within cochlear tissues. The results exhibited a notable decline in Apelin expression in the cochlear tissues of the Old group as opposed to the Young group, but after MSCs transplantation, Apelin expression was markedly upregulated in the Old group (Fig. S6C).

To further explore whether MSC-released EVs deliver Apelin to macrophages and regulate anti-inflammatory effects, we used lentivirus to silence or interfere with Apelin in MSC, followed by isolation of EVs and co-culturing with Ana-1 macrophages. The expression of Apelin in MSCs and EVs was found to be reduced in the sh-Apelin group as opposed to the sh-NC group, as indicated by the results. The subsequent experiments focused on the sh-Apelin-1 group displaying the most efficient knockdown (Fig. S6D-E). Meanwhile, based on the above experiments, we successfully established an inflammatory microenvironment in Ana-1 macrophages by stimulating them with LPS (Fig. 6A-E).

IF results showed a drop in the expression of M2 macrophages (CD206 +) in the EVs.sh-Apelin group in comparison to the EVs.sh-NC group, while an upregulation was noted in the expression of CD206 + positive cells in the EVs.oe-Apelin group in contrast with EVs.oe-NC group (Fig. 7A). In addition, we collected cell supernatants and used ELISA to detect the expression of M1 macrophage markers (IL-6 and IL-1β) and M2 macrophage markers (IL-10 and Arg1). The results showed upregulation of IL-6 and IL-1β expression and downregulation of IL-10 and Arg1 expression in EVs.sh-Apelin group contrasted with EVs.sh-NC group, while a significant reversal in the levels of these factors was detected in EVs.oe-Apelin group compared to EVs.oe-NC group (Fig. 7B).

Research conducted previously has indicated an increase in the ratio of M2 macrophages in older mice (Yamaguchi et al. 2020). Furthermore, the introduction of the accumulated EVs into the group of senior mice enabled the assessment of M1 and M2 macrophages' presence in the cochlear tissues via flow cytometry assessment. On comparison with the Old group, there was a decrease in the ratio of M1 macrophages (F4/80 + CD80 +) and an increase in the ratio of M2 macrophages (F4/80 + CD206 +) in the Old + EVs.sh-NC and Old + EVs.oe-NC categories, as outlined by the results. However, comparing to the Old + EVs.sh-NC group, the Old + EVs.sh-Apelin group exhibited a substantial increase in the ratio of M1 macrophages and a concomitant drop in the percentage of M2 macrophages. Similarly, relative to the Old + EVs.oe-NC group, the Old + EVs.oe-Apelin group revealed a remarkable decline in the proportion of M1 macrophages and a growth in the proportion of M2 macrophages (Fig. 7C-D). WB results further demonstrated that the levels of M2 macrophage-related proteins, Arg1 and IL-10, was upregulated in the cochlear tissues of Old + EVs.sh-NC and Old + EVs.oe-NC groups when juxtaposed with the Old group. However, the levels of these proteins substantially lowered in the Old + EVs.sh-Apelin group in contrast with the Old + EVs.sh-NC group, while they were substantially elevated in the Old + EVs.oe-Apelin group contrasted against the Old + EVs.oe-NC group (Fig. 7E). The discovery reinforces the close association between Apelin in MSC-derived EVs and M2 macrophage polarization.

In summary, our experimental results reveal the important role of MSC-released EVs in intercellular communication and inflammation regulation, which can promote M2 polarization and exert anti-inflammatory effects through targeted delivery of Apelin.

Protective effects of MSC-derived EVs with apelin on ARHL

The aging of cochlear hair cells is significantly influenced by the inflammatory response occurring within the inner ear. This process often involves the activation of immune cells and the secretion of inflammatory substances, which can detrimentally impact the integrity of cochlear hair cells, resulting

in oxidative harm, apoptosis, and decreased functional capabilities, culminating in the manifestation of auditory impairment (Wong and Ryan 2015).

In this experiment, we induced aging in the hair cells (HEI-OC1) through H_2O_2 induction in vitro and transfected MSCs with a lentivirus overexpressing Apelin. Subsequently, we collected EVs released by MSCs from different groups and co-cultured them with HEI-OC1 cells. We assessed the aging of HEI-OC1 cells through β-galactosidase staining (Fig. 8A). In contrast with the EVs.oe-NC + HEI-OC1 group, the degree of HEI-OC1 aging was noticeably lessened in the EVs.oe-Apelin + HEI-OC1 group, accompanied by downregulation of the aging-related proteins P53 and P21 (Fig. 8A-B), indicating that activating Apelin expression helps mitigate HEI-OC1 aging. Furthermore, we evaluated the vitality of HEI-OC1 cells applying the CCK8 assay. The results showed increased vitality of HEI-OC1 cells in the EVs.oe-Apelin + HEI-OC1 group compared to the EVs.oe-NC + HEI-OC1 group (Fig. 8C). AO staining experiments revealed a decreased apoptotic rate of HEI-OC1 cells in the EVs.oe-Apelin + HEI-OC1 group relative to the EVs.oe-NC + HEI-OC1 group (Fig. 8D).

Furthermore, we injected the collected EVs into the mice of the Old group and evaluated the ABR and DPOAE at the 1st, 2nd, and 4th weeks after treatment. Although no significant auditory improvement was observed in the 1st week of treatment, with extending treatment time, particularly in the 2nd and 4th weeks, the ABR thresholds significantly decreased, and DPOAE thresholds significantly increased in the Old + EVs.oe-NC and Old + EVs.oe-Apelin treatment groups compared to the Old group, indicating an improvement in auditory function. It is noteworthy that the Old mice were treated with Old + EVs.oe-Apelin showed more significant improvement in ABR and DPOAE tests compared to mice treated with Old + EVs.oe-NC alone (Fig. 8E-F).

In conclusion, our experimental results further emphasize the critical role of Apelin in MSC-derived EVs, which promotes M2 polarization, attenuates inflammation-induced HEI-OC1 aging and apoptosis, and significantly improves auditory function in aged mice. The discoveries propose the prospective clinical utility of MSC-derived EVs in protecting auditory function and preventing cochlear damage.

Discussion

Hearing loss is a common issue among the elderly population, and the existing treatment methods have certain limitations and challenges (Jiang et al. 2023, Lin et al. 2023, Anastasiadou and Al Khalili 2023). Currently, the main treatment methods include hearing aids and cochlear implants. However, these methods cannot fully restore hearing function, and for elderly individuals with hearing loss, there is a higher risk of surgery (Marx et al. 2021, Hunter et al. 2022, Peng et al. 2023). Therefore, it is necessary to seek new treatment methods to address this problem (Marrodan et al. 2021, Joshua et al. 2022, Tao et al. 2023) (Fig. 9).

In this study, scRNA-seq technology was used, which has the advantages of high resolution and sensitivity (Chen et al. 2020, Li et al. 2021). Compared to traditional RNA-seq and bulk RNA-seq, scRNA-seq can accurately analyze the transcriptome of individual cells, thus understanding the changes in different cell types (Beccuti and Calogero 2022, Alessandri and Calogero 2022). The use of this technology facilitates a deeper insight into the reasons for hearing impairment and the exploration of fresh therapeutic interventions (Xu et al. 2023).

This study found that the transplantation of MSCs can enhance auditory restoration in individuals suffering from auditory impairment. In comparison with other related studies, our research demonstrates the superiority of MSCs therapy in auditory recovery, which may be attributed to the multidifferentiation ability of MSCs and its regulation of inflammatory responses. Fresh perspectives and methodologies are introduced for the management of auditory impairment.

The research unveiled the significant involvement of EVs in modulating the inflamed microenvironment by transmitting Apelin. An innovative perspective is provided for understanding the mechanism related to hearing loss and discovering fresh therapeutic approaches. By comparing its role and effects with other regulatory factors in auditory recovery, we can better understand the mode of action and effectiveness of EVs in delivering Apelin.

Employing scRNA-seq, molecular biology techniques, and animal experiments, this research thoroughly scrutinized the involvement of MSCs and their EVs in promoting the recovery of auditory function in

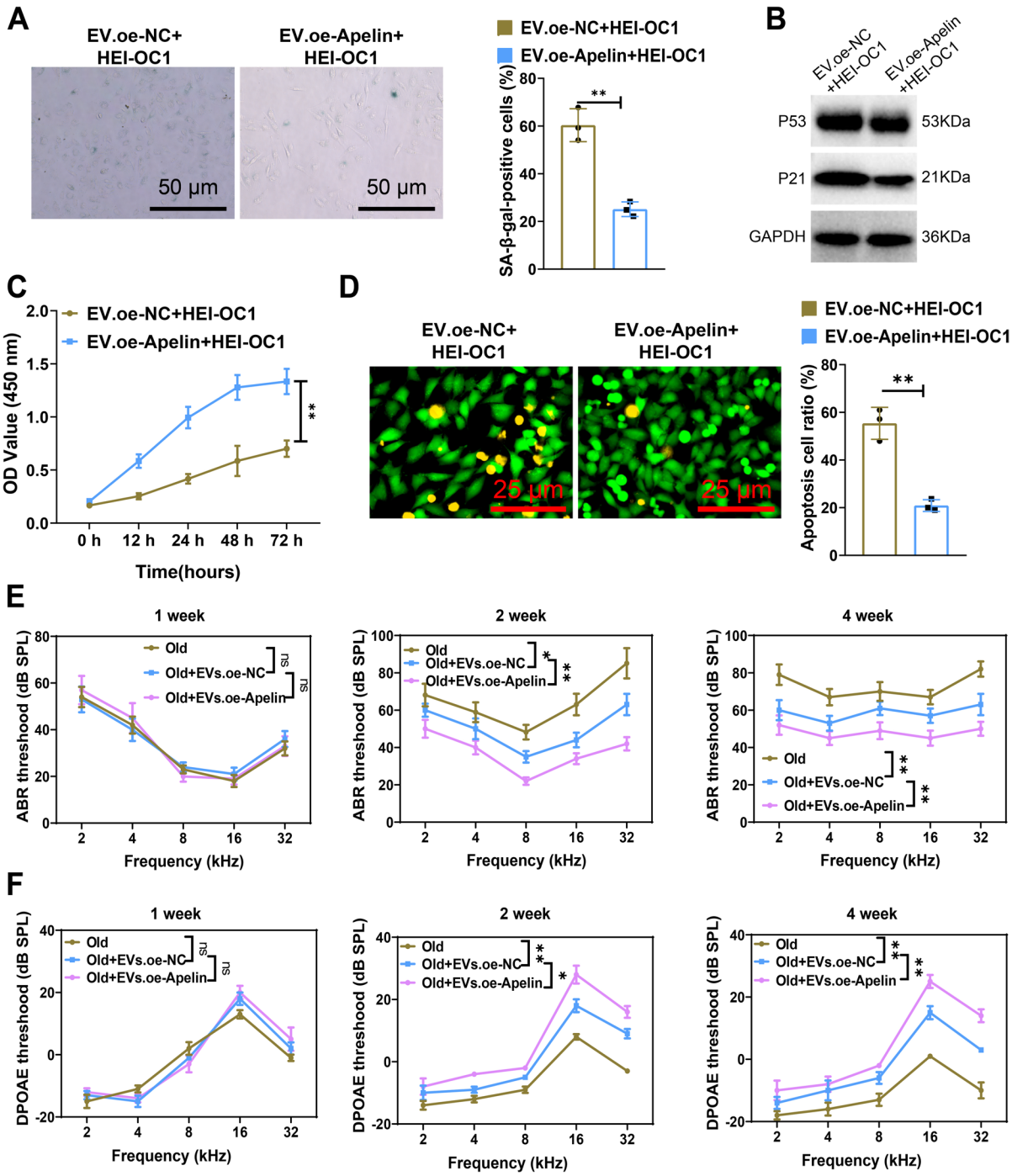

Fig. 8 MSC-derived EVs modified by apelin rescue cochlear cell senescence. Note: **A** β-galactosidase staining to detect cochlear cell senescence, Scale bar = 50 μm; **B** WB analysis of expression of senescence-related proteins P53 and P21; **C** CCK8 assay to measure cochlear cell viability; **D** AO staining to detect apoptosis in cochlear cells, apoptotic cells appear orange, while viable cells appear green, Scale bar = 25 μm; **E** ABR hearing threshold measurements in mice from different groups at different time points after EVs treatment; **F** DPOAE hearing threshold measurements in mice from different groups at different time points after EVs treatment. $^{**}P<0.01$, $^{*}P<0.05$, $^{ns}P>0.05$. Cell experiments were performed in triplicate, while animal experiments were $n=5$

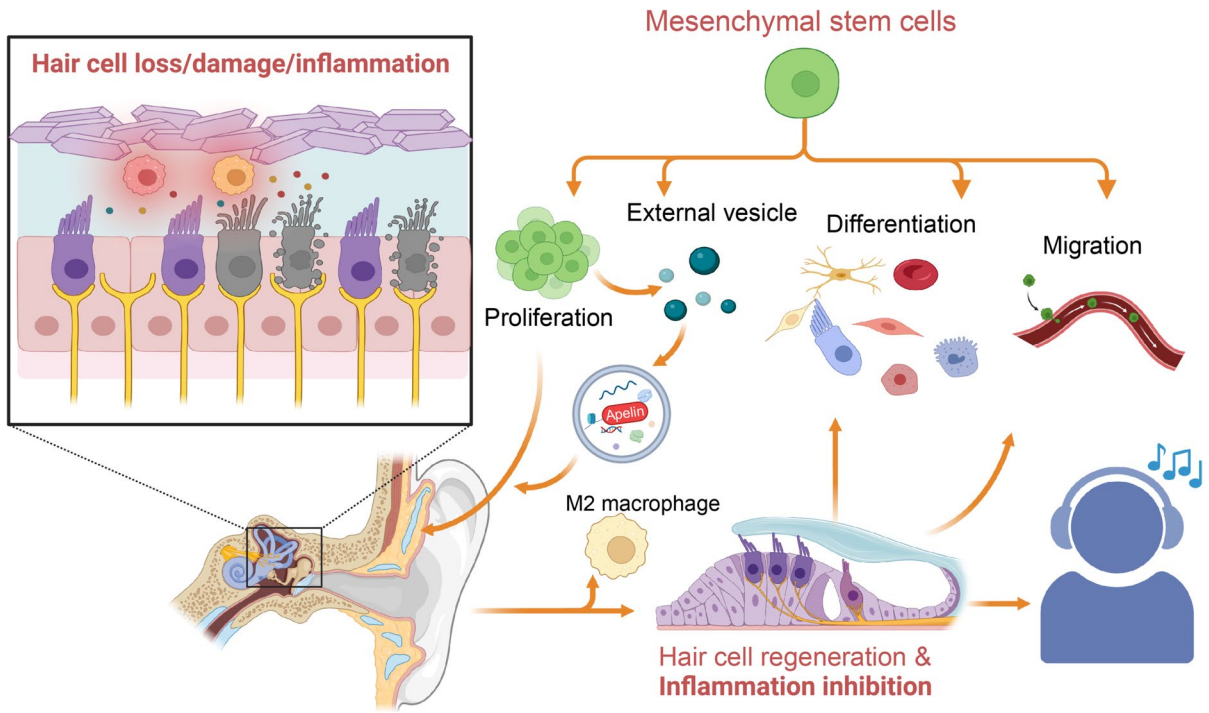

Fig. 9 Mechanism diagram illustrating how MSCs rescue hearing loss through repairing cochlear auditory cells and exerting anti-inflammatory effects by targeted delivery of Apelin and regulating M2 polarization

aged mice. The enhancement of elderly patients' life quality afflicted by auditory impairment is effectively achieved through the application of MSCs transplant to mend the hearing impairment.

Using scRNA-seq technology, the probable significance and molecular mechanisms concerning the therapeutic role of MSCs in ARHL are unveiled in this research. This research has significant scientific and clinical implications. Firstly, the study clarifies the relevance between MSCs and subpopulations of ear cells. Through single-cell transcriptomic analysis, researchers found that MSCs can differentiate into cell types closely related to auditory function, such as hair cells, Deiters cells, pillar cells, and inner phalangeal cells/inner border cells. This discovery provides a theoretical basis and new strategies for using MSCs to treat ARHL. Secondly, the study demonstrates that EVs derived from MSCs can redirect macrophages to the M2 phenotype through targeted delivery of Apelin, exerting an anti-inflammatory effect and salvaging hair cell vitality. The employment of vesicles in signaling introduces promising avenues for managing hearing impairment. By controlling the level and delivery mechanism of Apelin in EVs, it is possible to regulate inflammatory responses and hair cell degradation to promote hearing recovery. Additionally, in vivo experiments further confirm that the regeneration of auditory function in aged mice can be facilitated by the introduction of MSCs through transplantation, leading to the restoration of cochlear hair cells. The application of MSCs therapy in managing ARHL among the elderly is substantiated by compelling evidence.

Nevertheless, there are several constraints linked to this research. First, although scRNA-seq is highly advanced, data interpretation and cell subpopulation identification remain challenging. Second, this study only conducted experimental validation in an aged mouse model, and the mechanisms observed in young mice remain unknown. Additionally, additional research in clinical settings is necessary to validate its effectiveness and safety in human subjects. Deeper investigation in future studies could focus extensively on the mechanisms and effects of MSC-derived EVs delivering Apelin, as well as explore other potential molecular targets. Furthermore, clinical research on

the application of MSCs therapy for ARHL is crucial. By optimizing MSCs transplantation protocols, enhancing therapeutic efficacy, and combining it with other treatment modalities, such as gene therapy and pharmacological interventions, it may be possible to broaden the treatment options for ARHL.

Conclusions

In conclusion, this study demonstrates the therapeutic efficacy of MSCs transplantation and EV-mediated Apelin delivery for ARHL through comprehensive validations at the cellular and animal levels. Using scRNA-seq, we identified Apelin as a potential key target and revealed its regulatory role in the inflammatory microenvironment as a mechanism underlying MSC therapy. These findings go beyond a proof of concept by providing mechanistic insights into the therapeutic potential of MSCs and EVs. Nonetheless, significant challenges remain, including optimizing transplantation protocols and elucidating the precise mechanisms of EV-mediated Apelin delivery. Future studies will address these challenges to further refine the therapy and explore multimodal approaches to maximize treatment efficacy, paving the way for innovative advancements in ARHL treatment and related fields.

Acknowledgements Not applicable.

Author contribution Shengqun Xu and Dongliang Liu performed experiments and analyzed data. Fang Zhang led scRNA-seq analysis and interpretation. Yuan Tian supervised the study and revised the manuscript. All authors approved the final version.

Funding This work was supported by The Science Foundation of Liaoning Province (2023-MS-164).

Data availability The data that supports the findings of this study are available on request from the corresponding author.

Code availability Not applicable.

Declarations

Ethics approval The experimental procedures and animal handling protocols were approved by Shengjing Hospital of China Medical University Animal Ethics Committee.

Consent to participate Not applicable.

Consent for publication Not applicable.

Conflicts of interest The authors declare that they have no competing interests.

Consent for publication Consent for publication was obtained from the participants.

Competing interests The authors declare no competing interests.

References

Alessandri L, Calogero RA (2002) Functional-Feature-Based Data Reduction Using Sparsely Connected Autoencoders [Internet]. Methods in Molecular Biology. New York, NY: Springer US [cited 2024 Dec 24]. 231–40. https://doi.org/10.1007/978-1-0716-2756-3_11

Anastasiadou S, Al Khalili Y (2023) Hearing Loss. StatPearls. Treasure Island (FL): StatPearls Publishing

Bagheri E, Abnous K, Farzad SA, Taghdisi SM, Ramezani M, Alibolandi M (2020) Targeted doxorubicin-loaded mesenchymal stem cells-derived exosomes as a versatile platform for fighting against colorectal cancer [Internet]. Life Sciences. Elsevier BV; [cited 2024 Dec 24]. 118369. https://doi.org/10.1016/j.lfs.2020.118369

Baglio SR, Rooijers K, Koppers-Lalic D, Verweij FJ, Pérez Lanzón M, Zini N, et al (2015) Human bone marrow- and adipose-mesenchymal stem cells secrete exosomes enriched in distinctive miRNA and tRNA species [Internet]. Stem Cell Res Ther. Springer Science and Business Media LLC [cited 2024 Dec 24]. https://doi.org/10.1186/s13287-015-0116-z

Beccuti M, Calogero RA (2022) Single-Cell RNAseq Clustering [Internet]. Methods in Molecular Biology. New York, NY: Springer US [cited 2024 Dec 24]. p. 241–50. https://doi.org/10.1007/978-1-0716-2756-3_12

Bunnell BA (2021) Adipose Tissue-Derived Mesenchymal Stem Cells [Internet]. Cells. MDPI AG [cited 2024 Dec 24]. 3433. https://doi.org/10.3390/cells10123433

Cao L, Xu H, Wang G, Liu M, Tian D, Yuan Z (2019) Extracellular vesicles derived from bone marrow mesenchymal stem cells attenuate dextran sodium sulfate-induced ulcerative colitis by promoting M2 macrophage polarization [Internet]. Int Immunopharmacol. Elsevier BV [cited 2024 Dec 24]. p. 264–74. https://doi.org/10.1016/j.intimp.2019.04.020

Chen W, Jongkamonwiwat N, Abbas L, Eshtan SJ, Johnson SL, Kuhn S, et al (2012) Restoration of auditory evoked responses by human ES-cell-derived otic progenitors [Internet]. Nature. Springer Science and Business Media LLC [cited 2024 Dec 24]. p. 278–82. https://doi.org/10.1038/nature11415

Chen TN, Gupta A, Zalavadia MD, Streets A (2020) μCB-seq: microfluidic cell barcoding and sequencing for high-resolution imaging and sequencing of single cells [Internet]. Lab Chip. Royal Society of Chemistry (RSC) [cited 2024 Dec 24]. p. 3899–913. https://doi.org/10.1039/d0lc00169d

Chen P, Tang S, Li M, Wang D, Chen C, Qiu Y, et al (2022) Single-Cell and Spatial Transcriptomics Decodes Wharton's Jelly-Derived Mesenchymal Stem Cells Heterogeneity and a Subpopulation with Wound Repair Signatures [Internet]. Advanced Science. Wiley [cited 2024 Dec 24]. https://doi.org/10.1002/advs.202204786

Cho SI, Jo E-R, Song H (2022) Urolithin A attenuates auditory cell senescence by activating mitophagy [Internet]. Sci Rep. Springer Science and Business Media LLC [cited 2024 Dec 24]. https://doi.org/10.1038/s41598-022-11894-2

Cornejo-Sanchez DM, Li G, Fabiha T, Wang R, Acharya A, Everard JL, et al (2023) Rare-variant association analysis reveals known and new age-related hearing loss genes [Internet]. Eur J Hum Genet. Springer Science and Business Media LLC [cited 2024 Dec 24]. p. 638–47. https://doi.org/10.1038/s41431-023-01302-2

Di W, Fan W, Wu F, Shi Z, Wang Z, Yu M, et al (2021) Clinical characterization and immunosuppressive regulation of CD161 (KLRB1) in glioma through 916 samples [Internet]. Cancer Science. Wiley [cited 2024 Dec 24]. p. 756–69. https://doi.org/10.1111/cas.15236

Gao X, Bao W, Bai J, Fan K, Li L, Li Y (2022) UHMK1 aids colorectal cancer cell proliferation and chemoresistance through augmenting IL-6/STAT3 signaling [Internet]. Cell Death Dis. Springer Science and Business Media LLC [cited 2024 Dec 24]. https://doi.org/10.1038/s41419-022-04877-8

Ge J, Geng S, Gao Y, Ren G, Sun X, Jiang H (2023) Construction and Effect of the Three-Level and Two-Stage Screening Mode for Age-Related Hearing Loss: A Study Based on the Community in Shanghai, China [Internet]. CIA. Informa UK Limited [cited 2024 Dec 24]. p. 1309–20. https://doi.org/10.2147/cia.s423822

Gruver A, Hudson L, Sempowski G (2007) Immunosenescence of ageing [Internet]. The Journal of Pathology. Wiley [cited 2024 Dec 24]. p. 144–56. https://doi.org/10.1002/path.2104

Hade MD, Suire CN, Mossell J, Suo Z (2022) Extracellular vesicles: Emerging frontiers in wound healing [Internet]. Medicinal Research Reviews. Wiley [cited 2024 Dec 24]. p. 2102–25. https://doi.org/10.1002/med.21918

Hao Y, Hao S, Andersen-Nissen E, Mauck WM III, Zheng S, Butler A, et al. (2021) Integrated analysis of multimodal single-cell data [Internet]. Cell. Elsevier BV [cited 2024 Dec 24]. p. 3573–3587.e29. https://doi.org/10.1016/j.cell.2021.04.048

He Z-H, Li M, Fang Q-J, Liao F-L, Zou S-Y, Wu X, et al. (2021) FOXG1 promotes aging inner ear hair cell survival through activation of the autophagy pathway [Internet]. Autophagy. Informa UK Limited [cited 2024 Dec 24]. p. 4341–62. https://doi.org/10.1080/15548627.2021.1916194

Hoang DM, Pham PT, Bach TQ, Ngo ATL, Nguyen QT, Phan TTK, et al. (2022) Stem cell-based therapy for human diseases [Internet]. Sig Transduct Target Ther. Springer Science and Business Media LLC [cited 2024 Dec 24]. https://doi.org/10.1038/s41392-022-01134-4

Holm TH, Lykke-Hartmann K (2016) Insights into the Pathology of the α3 Na+/K+-ATPase Ion Pump in Neurological Disorders; Lessons from Animal Models [Internet]. Front Physiol Frontiers Media SA [cited 2024 Dec 24]. https://doi.org/10.3389/fphys.2016.00209

Hu Q, Lyon CJ, Fletcher JK, Tang W, Wan M, Hu TY (2021) Extracellular vesicle activities regulating macrophage- and tissue-mediated injury and repair responses [Internet]. Acta Pharm Sin B. Elsevier BV [cited 2024 Dec 24]. p. 1493–512. https://doi.org/10.1016/j.apsb.2020.12.014

Hunter JB, Yancey KL, Lee KH (2022) Pediatric Single-Sided Deafness [Internet]. Otolaryngol Cli North Am. Elsevier BV [cited 2024 Dec 24]. p. 1139–49. https://doi.org/10.1016/j.otc.2022.07.003

Jeon S-J, Oshima K, Heller S, Edge ASB (2007) Bone marrow mesenchymal stem cells are progenitors in vitro for inner ear hair cells [Internet]. Mol Cell Neurosci. Elsevier BV [cited 2024 Dec 24]. p. 59–68. https://doi.org/10.1016/j.mcn.2006.10.003

Jiang F, Mishra SR, Shrestha N, Ozaki A, Virani SS, Bright T, et al (2023) RETRACTED: Association between hearing aid use and all-cause and cause-specific dementia: an analysis of the UK Biobank cohort [Internet]. Lancet Public Health. Elsevier BV [cited 2024 Dec 24]. e329–38. https://doi.org/10.1016/s2468-2667(23)00048-8

Joshua TG, Ayub A, Wijesinghe P, Nunez DA (2022) Hyperbaric Oxygen Therapy for Patients With Sudden Sensorineural Hearing Loss [Internet]. JAMA Otolaryngol Head Neck Surg. American Medical Association (AMA) [cited 2024 Dec 24]. p. 5. https://doi.org/10.1001/jamaoto.2021.2685

Kanzaki S, Toyoda M, Umezawa A, Ogawa K (2020) Application of Mesenchymal Stem Cell Therapy and Inner Ear Regeneration for Hearing Loss: A Review [Internet]. IJMS. MDPI AG [cited 2024 Dec 24]. p. 5764. https://doi.org/10.3390/ijms21165764

Koh J-Y, Affortit C, Ranum PT, West C, Walls WD, Yoshimura H, et al (2023). Single-cell RNA-sequencing of stria vascularis cells in the adult Slc26a4-/- mouse [Internet]. BMC Med Genomics. Springer Science and Business Media LLC [cited 2024 Dec 24]. https://doi.org/10.1186/s12920-023-01549-0

Leeper NJ, Tedesco MM, Kojima Y, Schultz GM, Kundu RK, Ashley EA, et al (2009) Apelin prevents aortic aneurysm formation by inhibiting macrophage inflammation [Internet]. Am J Physiol-Heart Circ Physiol. American Physiological Society [cited 2024 Dec 24]. p. H1329–35. https://doi.org/10.1152/ajpheart.01341.2008

Leong S, Teh BM, Kim AH (2023) Characterization of otologic symptoms appearing after COVID-19 vaccination [Internet]. Am J Otolaryngol. Elsevier BV [cited 2024 Dec 24]. 103725. https://doi.org/10.1016/j.amjoto.2022.103725

Li P, Xin H, Lu L. Extracellular vesicle-encapsulated microRNA-424 exerts inhibitory function in ovarian cancer by targeting MYB. J Transl Med. 2021;19(4). Springer Science and Business Media LLC. https://doi.org/10.1186/s12967-020-02652-x.

Li Q-C, Li C, Zhang W, Pi W, Han N (2022) Potential Effects of Exosomes and their MicroRNA Carrier on Osteoporosis [Internet]. CPD. Bentham Science Publishers Ltd. [cited 2024 Dec 24]. p. 899–909. https://doi.org/10.2174/1381612828666220128104206

Li C, Guan N, Liu F (2023) T7 peptide-decorated exosome-based nanocarrier system for delivery of Galectin-9 siRNA to stimulate macrophage repolarization in glioblastoma [Internet]. J Neurooncol. Springer Science and Business Media LLC [cited 2024 Dec 24]. 93–108. https://doi.org/10.1007/s11060-023-04257-y

Lin H, Xiong H, Su Z, Pang J, Lai L, Zhang H, et al (2019). Inhibition of DRP-1-Dependent Mitophagy Promotes Cochlea Hair Cell Senescence and Exacerbates Age-Related Hearing Loss [Internet]. Front Cell Neurosci Frontiers Media SA [cited 2024 Dec 24]. https://doi.org/10.3389/fncel.2019.00550

Lin FR, Pike JR, Albert MS, Arnold M, Burgard S, Chisolm T, et al (2023) Hearing intervention versus health education control to reduce cognitive decline in older adults with hearing loss in the USA (ACHIEVE): a multicentre, randomised controlled trial [Internet]. The Lancet. Elsevier BV [cited 2024 Dec 24]. p. 786–97. https://doi.org/10.1016/s0140-6736(23)01406-x

Liu W, Molnar M, Garnham C, Benav H, Rask-Andersen H (2018). Macrophages in the Human Cochlea: Saviors or Predators—A Study Using Super-Resolution Immunohistochemistry [Internet]. Front Immunol Front Media SA [cited 2024 Dec 24]. https://doi.org/10.3389/fimmu.2018.00223

Liu J, Qiu X, Lv Y, Zheng C, Dong Y, Dou G, et al (2020) Apoptotic bodies derived from mesenchymal stem cells promote cutaneous wound healing via regulating the functions of macrophages [Internet]. Stem Cell Res Ther. Springer Science and Business Media LLC [cited 2024 Dec 24]. https://doi.org/10.1186/s13287-020-02014-w

Ma L, Hernandez MO, Zhao Y, Mehta M, Tran B, Kelly M, et al. Tumor cell biodiversity drives microenvironmental reprogramming in liver cancer. Cancer Cell. 2019;36(4):418–30.e6. Elsevier BV. https://doi.org/10.1016/j.ccell.2019.08.007.

Ma P, Amemiya HM, He LL, Gandhi SJ, Nicol R, Bhattacharyya RP, et al. (2023) Bacterial droplet-based single-cell RNA-seq reveals antibiotic-associated heterogeneous cellular states [Internet]. Cell. Elsevier BV [cited 2024 Dec 24]. p. 877–891.e14. https://doi.org/10.1016/j.cell.2023.01.002

Mahmoudi S, Mancini E, Xu L, Moore A, Jahanbani F, Hebestreit K, et al (2019) Heterogeneity in old fibroblasts is linked to variability in reprogramming and wound healing [Internet]. Nature. Springer Science and Business Media LLC [cited 2024 Dec 24]. p. 553–8. https://doi.org/10.1038/s41586-019-1658-5

Marrodan M, Fiol MP, Correale J (2021) Susac syndrome: challenges in the diagnosis and treatment [Internet]. Brain. Oxford University Press (OUP) [cited 2024 Dec 24]. p. 858–71. https://doi.org/10.1093/brain/awab476

Marx M, Mosnier I, Venail F, Mondain M, Uziel A, Bakhos D, et al (2021) Cochlear Implantation and Other Treatments in Single-Sided Deafness and Asymmetric Hearing Loss: Results of a National Multicenter Study Including a Randomized Controlled Trial [Internet]. Audiol Neurotol. S. Karger AG [cited 2024 Dec 24]. p. 414–24. https://doi.org/10.1159/000514085

Niknazar S, Abbaszadeh H-A, Peyvandi H, Rezaei O, Forooghirad H, Khoshsirat S, et al (2019). Protective effect of [Pyr1]-apelin-13 on oxidative stress-induced apoptosis in hair cell-like cells derived from bone marrow mesenchymal stem cells [Internet]. European J Pharmacol. Elsevier BV [cited 2024 Dec 24]. 25–32. https://doi.org/10.1016/j.ejphar.2019.03.012

Noble KV, Liu T, Matthews LJ, Schulte BA, Lang H (2019) Age-Related Changes in Immune Cells of the Human Cochlea [Internet]. Front Neurol. Frontiers Media SA [cited 2024 Dec 24]. https://doi.org/10.3389/fneur.2019.00895

Peng ZE, Garcia A, Godar SP, Holt JR, Lee DJ, Litovsky RY (2023) Hearing Preservation and Spatial Hearing Outcomes After Cochlear Implantation in Children With TMPRSS3 Mutations [Internet]. Otol Neurotol. Ovid Technologies (Wolters Kluwer Health) [cited 2024 Dec 24]. p. 21–5. https://doi.org/10.1097/mao.0000000000003747

Petitpré C, Faure L, Uhl P, Fontanet P, Filova I, Pavlinkova G, et al (2022) Single-cell RNA-sequencing analysis of the developing mouse inner ear identifies molecular logic of auditory neuron diversification [Internet]. Nat Commun. Springer Science and Business Media LLC [cited 2024 Dec 24]. https://doi.org/10.1038/s41467-022-31580-1

Piekna-Przybylska D, Na D, Zhang J, Baker C, Ashton JM, White PM (2023) Single cell RNA sequencing analysis of mouse cochlear supporting cell transcriptomes with activated ERBB2 receptor indicates a cell-specific response that promotes CD44 activation [Internet]. Front Cell Neurosci Front Media SA [cited 2024 Dec 24]. https://doi.org/10.3389/fncel.2022.1096872

Pouraghaei S, Moztarzadeh F, Chen C, Ansari S, Moshaverinia A (2020) Microenvironment Can Induce Development of Auditory Progenitor Cells from Human Gingival Mesenchymal Stem Cells [Internet]. ACS Biomater Sci Eng American Chemical Society (ACS) [cited 2024 Dec 24]. p. 2263–73. https://doi.org/10.1021/acsbiomaterials.9b01795

Qin T, Zhang G, Zheng Y, Li S, Yuan Y, Li Q, et al (2023) A population of stem cells with strong regenerative potential discovered in deer antlers [Internet]. Science. American

Association for the Advancement of Science (AAAS) [cited 2024 Dec 24]. 840–7. https://doi.org/10.1126/science.add0488

Ragni E, Palombella S, Lopa S, Talò G, Perucca Orfei C, De Luca P, et al (2020) Innovative Visualization and Quantification of Extracellular Vesicles Interaction with and Incorporation in Target Cells in 3D Microenvironments [Internet]. Cells. MDPI AG [cited 2024 Dec 24]. 1180. https://doi.org/10.3390/cells9051180

Sanchez HA, Verselis VK (2014) Aberrant Cx26 hemichannels and keratitis-ichthyosis-deafness syndrome: insights into syndromic hearing loss [Internet]. Front Cell Neurosci Front Media SA [cited 2024 Dec 24]. https://doi.org/10.3389/fncel.2014.00354

Seicol BJ, Lin S, Xie R (2022) Age-Related Hearing Loss Is Accompanied by Chronic Inflammation in the Cochlea and the Cochlear Nucleus [Internet]. Front Aging Neurosci Front Media SA [cited 2024 Dec 24]. https://doi.org/10.3389/fnagi.2022.846804

Sun G, Zheng Y, Fu X, Zhang W, Ren J, Ma S, et al (2022) Single-cell transcriptomic Atlas of mouse cochlear aging [Internet]. Protein Cell. Springer Science and Business Media LLC [cited 2024 Dec 24]. https://doi.org/10.1093/procel/pwac058

Tajima S, Danzaki K, Ikeda K, Kamiya K (2020) Degradation and modification of cochlear gap junction proteins in the early development of age-related hearing loss [Internet]. Exp Mol Med. Springer Science and Business Media LLC [cited 2024 Dec 24]. p. 166–75. https://doi.org/10.1038/s12276-020-0377-1

Takeda H, Dondzillo A, Randall JA, Gubbels SP (2021) Selective ablation of cochlear hair cells promotes engraftment of human embryonic stem cell-derived progenitors in the mouse organ of Corti [Internet]. Stem Cell Res Ther. Springer Science and Business Media LLC [cited 2024 Dec 24]. https://doi.org/10.1186/s13287-021-02403-9

Tang F, Li J, Qi L, Liu D, Bo Y, Qin S, et al (2023) A pan-cancer single-cell panorama of human natural killer cells [Internet]. Cell. Elsevier BV [cited 2024 Dec 24]. p. 4235–4251.e20. https://doi.org/10.1016/j.cell.2023.07.034

Tao Y, Lamas V, Du W, Zhu W, Li Y, Whittaker MN, et al (2023) Treatment of monogenic and digenic dominant genetic hearing loss by CRISPR-Cas9 ribonucleoprotein delivery in vivo [Internet]. Nat Commun. Springer Science and Business Media LLC [cited 2024 Dec 24]. https://doi.org/10.1038/s41467-023-40476-7

Uchida Y, Sugiura S, Nishita Y, Saji N, Sone M, Ueda H (2019) Age-related hearing loss and cognitive decline — The potential mechanisms linking the two [Internet]. Auris Nasus Larynx. Elsevier BV [cited 2024 Dec 24]. p. 1–9. https://doi.org/10.1016/j.anl.2018.08.010

Verschuur C, Agyemang-Prempeh A, Newman TA (2014) Inflammation is associated with a worsening of presbycusis: Evidence from the MRC national study of hearing [Internet]. Int J Audiol. Informa UK Limited [cited 2024 Dec 24]. p. 469–75. https://doi.org/10.3109/14992027.2014.891057

Wang J, Liu X, Qiu Y, Shi Y, Cai J, Wang B, et al (2018) Cell adhesion-mediated mitochondria transfer contributes to mesenchymal stem cell-induced chemoresistance on T cell acute lymphoblastic leukemia cells [Internet]. J Hematol Oncol. Springer Science and Business Media LLC [cited 2024 Dec 24]. https://doi.org/10.1186/s13045-018-0554-z

Wang Y, Zhang L, Wu G-R, Zhou Q, Yue H, Rao L-Z, et al (2021) MBD2 serves as a viable target against pulmonary fibrosis by inhibiting macrophage M2 program [Internet]. Sci. Adv. American Association for the Advancement of Science (AAAS) [cited 2024 Dec 24]. https://doi.org/10.1126/sciadv.abb6075

Wang X, Zhang L, Li P, Zheng Y, Yang Y, Ji S (2022) Apelin/APJ system in inflammation [Internet]. International Immunopharmacology. Elsevier BV [cited 2024 Dec 24]. 108822. https://doi.org/10.1016/j.intimp.2022.108822

Watson N, Ding B, Zhu X, Frisina RD (2017) Chronic inflammation – inflammaging – in the ageing cochlea: A novel target for future presbycusis therapy [Internet]. Ageing Res Rev. Elsevier BV [cited 2024 Dec 24]. p. 142–8. https://doi.org/10.1016/j.arr.2017.10.002

Wei Z, Chen Z, Zhao Y, Fan F, Xiong W, Song S, et al (2021) Mononuclear phagocyte system blockade using extracellular vesicles modified with CD47 on membrane surface for myocardial infarction reperfusion injury treatment [Internet]. Biomaterials. Elsevier BV [cited 2024 Dec 24]. 121000. https://doi.org/10.1016/j.biomaterials.2021.121000

Weng Z, Wang Y, Ouchi T, Liu H, Qiao X, Wu C, et al (2022) Mesenchymal Stem/Stromal Cell Senescence: Hallmarks, Mechanisms, and Combating Strategies [Internet]. Stem Cells Translational Medicine. Oxford University Press (OUP) [cited 2024 Dec 24]. p. 356–71. https://doi.org/10.1093/stcltm/szac004

Wong ACY, Ryan AF (2015) Mechanisms of sensorineural cell damage, death and survival in the cochlea [Internet]. Front Aging Neurosci. Frontiers Media SA [cited 2024 Dec 24]. https://doi.org/10.3389/fnagi.2015.00058

Xu L, Wang X, Li J, Chen L, Wang H, Xu S, et al (2023) A novel PLS1 c.981+1G>A variant causes autosomal-dominant hereditary hearing loss in a family [Internet]. Clinical Genetics. Wiley [cited 2024 Dec 24]. p. 413–23. https://doi.org/10.1111/cge.14283

Yamaguchi Y, Kaida K, Suenaga Y, Ishigami A, Kobayashi Y, Nagata K (2020) Age-related dysfunction of p53-regulated phagocytic activity in macrophages [Internet]. Biochem Biophys Re Commun. Elsevier BV [cited 2024 Dec 24]. p. 462–6. https://doi.org/10.1016/j.bbrc.2020.05.121

Yang Z, Zhang Y, Yang S, Ding Y, Qu Y (2022) Low-Dose Resveratrol Inhibits RIPK3-Mediated Necroptosis and Delays the Onset of Age-Related Hearing Loss [Internet]. Front Pharmacol Front Media SA [cited 2024 Dec 24]. https://doi.org/10.3389/fphar.2022.910308

Yang Y, Lang P, Zhang X, Wu X, Cao S, Zhao C, et al. Molecular characterization of extracellular vesicles derived from follicular fluid of women with and without PCOS: integrating analysis of differential miRNAs and proteins reveals vital molecules involving in PCOS. J Assist Reprod Genet. 2023;40:537–52. Springer Science and Business Media LLC. https://doi.org/10.1007/s10815-023-02724-z.

Yun TJ, Igarashi S, Zhao H, Perez OA, Pereira MR, Zorn E, et al (2021) Human plasmacytoid dendritic cells mount a distinct antiviral response to virus-infected cells [Internet]. Sci. Immunol. American Association for the Advancement of Science (AAAS) [cited 2024 Dec 24]. https://doi.org/10.1126/sciimmunol.abc7302

Zhang Q-F, Li J, Jiang K, Wang R, Ge J, Yang H, et al (2020) CDK4/6 inhibition promotes immune infiltration in

ovarian cancer and synergizes with PD-1 blockade in a B cell-dependent manner [Internet]. Theranostics. Ivyspring International Publisher [cited 2024 Dec 24]. p. 10619–33. https://doi.org/10.7150/thno.44871

Zhao R, Yue T, Xu Z, Zhang Y, Wu Y, Bai Y, et al (2023) Electroencephalogram-based objective assessment of cognitive function level associated with age-related hearing loss [Internet]. GeroScience. Springer Science and Business Media LLC [cited 2024 Dec 24]. p. 431–46. https://doi.org/10.1007/s11357-023-00847-w

Zheng M, Yan J, Hao W, Ren Y, Zhou M, Wang Y, et al (2022) Worsening hearing was associated with higher β-amyloid and tau burden in age-related hearing loss [Internet]. Sci Rep. Springer Science and Business Media LLC [cited 2024 Dec 24]. https://doi.org/10.1038/s41598-022-14466-6

Zhi L, Zhao L, Zhang X, Liu W, Gao B, Wang F, et al (2021) SLCO1B3 promotes colorectal cancer tumorigenesis and metastasis through STAT3 [Internet]. Aging Impact J, LLC; [cited 2024 Dec 24]. 22164–75. https://doi.org/10.18632/aging.203502

Zhou Y, Wang G, Cai J, Du Y, Li H, Duan L, et al (2023) Exosomal transfer of miR-195–5p restrains lung adenocarcinoma progression [Internet]. Exp Cell Res. Elsevier BV [cited 2024 Dec 24]. 113485. https://doi.org/10.1016/j.yexcr.2023.113485